In vivo and *in vitro* strategies to study precise gene editing using CRISPR-Cas9

Jacob Conradi

Thesis submitted for the degree of Master of Science in Molecular Bioscience and Biochemistry
60 credits

Department of Bioscience
Faculty of Mathematics and Natural Sciences

UNIVERSITY OF OSLO

June 2022

Acknowledgements

The work presented in this thesis was conducted at Center for Molecular Medicine Norway (NCMM), Oslo from June 2021 to June 2022 under the supervision of Emma Haapaniemi, Pavel Kopcil and Hans-Petter Hersleth.

First and foremost, I want to thank my main supervisor Emma Haapaniemi for having me as a student in her research group. Thank you to all members of the Haapaniemi group for creating a good workspace. You have all been very welcoming and helpful. It has been a pleasure to be part of your lab and I feel privileged to have been conducting my master thesis within such an exciting field of science in the company of highly knowledgeable and encouraging people. A special thanks goes to my daily supervisor Pavel Kopcil for everything he has thought me and his guidance through the whole research process. I also want to thank my internal supervisor at UiO, Hans-Petter Hersleth for guidance relevant to writing a thesis.

Finally, I want to thank my friends and family for all their support and motivation throughout my master thesis.

Summary

Introduction of designed DNA templates by the CRISPR-Cas9 gene-editing system relies on homology-directed DNA repair (HDR). Preferentially, cells repair DNA double-strand breaks (DBS) by the fast, template-free, and error-prone mechanism of non-homologous end joining (NHEJ). Promoting HDR will allow more precise gene editing by CRISPR-Cas9, which can be applied to clinical purposes of treating monogenic immune diseases in children, including severe combined immunodeficiency (SCID). Such diseases can also be treated by hematopoietic stem cell transplantation (HSCT) from a healthy donor or genetically engineered HSCTs derived from the patient themselves. HSCT is complex, as a mismatch of the HLA of the donor and recipient causes allograft rejection.

In this master thesis, we evaluated human engraftment of *ADA2*-edited or unedited hematopoietic stem and progenitor cells (HSPCs) in the NSG mouse model. Additionally, we assess the effects of various HDR enhancers on tilting the balance between HDR pathway over NHEJ pathway in primary human healthy donor fibroblast cells.

We observed moderate to high human engraftment 12 weeks post-injection in mouse bone marrow (~60-70%). We found HDR enhancers co-delivered as mRNA did not promote higher HDR editing outcome in fibroblast cells using ssODN repair template in the *ADA2* disease relevant mutation locus C→T (R169Q). Thus, further experiments are needed to optimize gene therapy to treat monogenic immune diseases.

Abbreviations

ADA	Adenosine deaminase
Ad5	Adenovirus-5-E4orf6/7
APC	Antigen-presenting cell
CRISPR	Clustered regulatory interspaced short palindromic repeats
Cry1	Cryptochrome 1
CTL	cytotoxic T cells
CYREN	Cell cycle regulator of non-homologous end-joining
DC	Dendritic cell
ddPCR	Digital droplet polymerase chain reaction
DEG	Diethylene glycol
DSB	Double-strand break
EGFP	Enhanced green fluorescent protein
FE mice	Finished-experiment mice
gRNA	guide RNA
GSE56	Genetic suppressor element 56
GvHD	Graft-versus-host-disease
HDR	Homology-directed DNA repair
HLA	Human leukocyte antigen
HSC	Hematopoietic stem cells
HSCT	Hematopoietic stem cell transplantation
HSPC	Hematopoietic stem and progenitor cells
IVT	In vitro transcription
I53	inhibition of 53BP1
LT-HSC	Long term Hematopoietic stem cells
MCH	Major histocompatibility complex
MDU	Minimal disease unit
mRNA	messenger RNA
NK Cells	Natural killer cells
NHEJ	Non-homologous end-joining

NSG	NOD SCID gamma™
PAM	Protospacer adjacent motif
PBMC	Peripheral blood mononuclear cell
RNP	Ribonucleoprotein
sgRNA	single-guide RNA
ST-HSC	Short term Hematopoietic stem cells
ssODN	Single strand oligodeoxynucleotides
SCID	Severe combined immunodeficiencies
TALEN	Transcription activator-like effector nuclease
TH Cells	T helper cells
UE mice	Unfinished-experiment mice
ZFN	Zinc-finger nuclease
53BP1	p53 binding protein 1

Table of content

1. Introduction

Hematological pathologies are diseases affecting the cells of the blood and immune system, including blood malignancies, immunodeficiencies, and genetic disorders such as severe combined immunodeficiencies (SCID) [1]. Many such diseases arise from abnormalities in the hematopoietic stem cells (HSC) which are the origin of all cells in the hematopoietic system. To this day, no definite cure is clinically available to patients suffering health impeding genetic hematological disorders. These patients are suited for gene therapy and hematopoietic stem cell transplantation (HSCT), but there are still many limitations to the application of these treatments. [2]

1.1 Hierarchy of Human Hematopoietic Cells

HSCs are multipotent cells that reside in the bone marrow and have both the potential to differentiate into specialized blood cells in a process known as hematopoiesis and the ability of self-renewal. Through self-renewal, the HSCs ensure the HSC pool size is maintained in the bone marrow compartment at the same time as blood cells are generated [3]. Self-renewing HSCs are found in a specific microenvironment called the niche and are subdivided into long-term HSCs (LT-HSCs) and short-term HSCs (ST-HSCs) [4]. As implied by the name, ST-HSCs have limited self-renewing capacity (<1 month) and are destined to differentiate into blood cells [5]. LT-HSCs have long-term self-renewal capacity (>3-4 months) and will differentiate into ST-HSCs. The population of LT-HSC is rare but can be distinguished from ST-HSCs by the expression of various surface markers, including CD34, CD38, CD90, and CD45RA [3].

Once the differentiation process is initiated, the ST-HSC leaves the niche and loses its ability to self-renew [4]. HSC can also differentiate into two kinds of multipotent progenitor cells, either common myeloid progenitors or common lymphoid progenitors. Cells committed to the lymphoid lineage will differentiate into T- or B- lymphocytes, which are the cells constituting adaptive immunity, or natural killer cells (NK cells), which are involved in the innate immune response. B lymphocytes can differentiate into plasma cells, which will secrete antibodies to neutralize harmful pathogens or unhealthy cells [6]. Myeloid progenitors will have one of many fates. They can differentiate into red blood cells, such as platelets or oxygen-carrying erythrocytes. Alternatively, they can choose the path toward myeloid cells, which are white blood cells and the main attributers

of innate immunity. Such cells include macrophages, dendritic cells (DC), and granulocytes (Figure 1) [3].

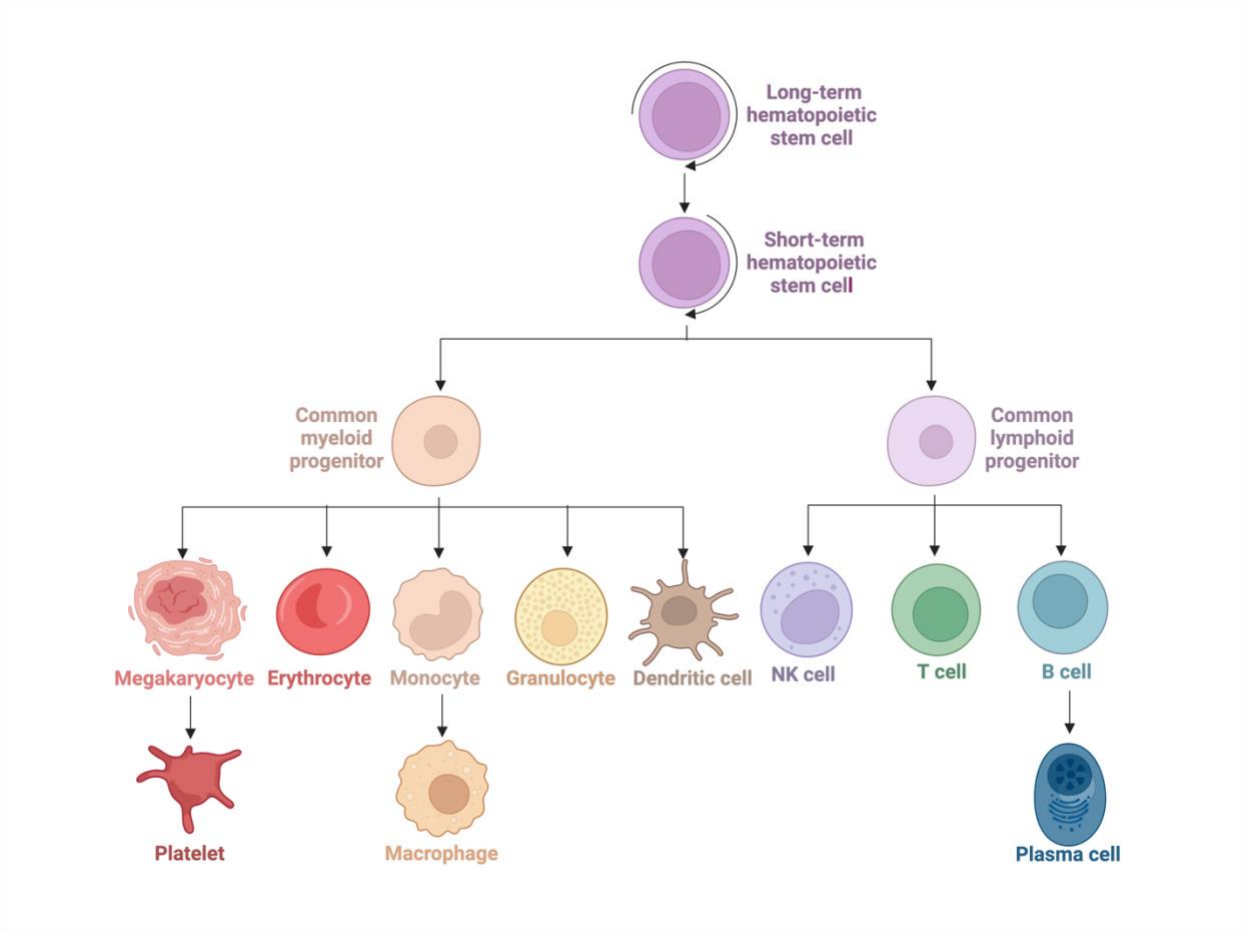

Figure 1: Schematic representation of the hematopoietic hierarchy

Long-term self-renewing hematopoietic stem cells (LT-HSC) differentiate into short-term self-renewing hematopoietic stem cells (ST-HSC). ST-HSC differentiate into either a common myeloid progenitor cell or a common lymphoid progenitor cell. Common myeloid progenitor cells can become (from the left) megakaryocytes that differentiate into platelets, erythrocytes, monocytes that differentiate into macrophages, granulocytes (which include eosinophils, neutrophils, and basophils (not shown)), or dendritic cells. Common lymphoid progenitor cells can become natural killer cells (NK cells), T cells, or B cells. B cells can differentiate into plasma cells. The figure was made with inspiration from [3]. Created in BioRender.com.

1.2 The Immunologic Aspect of Hematology

Our body is a complex system controlled by HSC-derived cells, the proteins they produce, and the environment surrounding them. Thoroughly managed responses provided by the immune system prevent us from getting infections and cancer. Our immune system is a collective and coordinated response to foreign substances, and it can be divided into innate immunity and adaptive immunity. The innate immune system is not specific but is the first immune response with the task of preventing, controlling, or eliminating pathogens such as viruses, bacteria, and fungi. The skin and mucosal surfaces are the first barriers of the immune system which the pathogen must overcome, before being faced with the complement system. Complement activation will swiftly recruit specialized phagocytes and other leukocytes from the blood to the infected area to destroy the pathogens in a process called inflammation. Not all pathogenic agents can be concurred by the innate system alone and this is why the course of vertebrate evolution has led to the emergence of the adaptive immune system [7].

A response by the adaptive immune system takes longer to develop and is provided by specialized cells called lymphocytes. Lymphocytes express diverse antigen receptors designed to specifically recognize the pathogen-infected cells. The diversity of these antigen receptors is generated when activation signals from cell surface receptors initiate lymphocyte cell maturation, which leads to rearrangement of the antigen receptor in addition to stimulating proliferation. The selection of lymphocytes with antigen receptors that are highly specific for non-self-antigens happens as part of the maturation and activation process. This is important so the immune system doesn't attack healthy cells and tissue of its own body [7].

1.2.1 Cooperation Between Immune Cells

After differentiation from HSCs in the bone marrow, B cell precursors migrate to the lymph nodes and T cell precursors to the thymus, where they will mature and become antigen specific. Together, T cells and B cells make up most of the adaptive immunity, which is divided into humoral immunity and cell-mediated immunity [7].

The humoral immune response is driven by the antibodies secreted by plasma cells [8], which coat pathogens to neutralize or mark for destruction provided by phagocytic cells, such as macrophages

[9]. Plasma cells are activated when an antigen is recognized by the B-cell receptor, an antibody expressed on the surface of the plasma cell [7]. Most of the time, antigens are not sufficient to activate the plasma cell [8]. Stimulation from a specific linage of T cells, CD4+ helper-T cells (TH cell), is needed for a complete activation. Before the TH cell can activate the plasma cell, it must first be activated itself by a professional antigen-presenting cell (APC). Dendritic cells are the most efficient APCs. They will capture and digest antigens to present a part of it to a T cell on a major histocompatibility complex class 2 (MHC II), enabling the naïve T cell to differentiate into a CD4+ TH cell. The antigen and the MHC II expressed on the DC are recognized by the T-cell receptor (TCR) on the surface of the T cell. In addition, costimulatory signals from the APC are needed for differentiation into TH cells. Cells that are presented with an antigen but don't receive signals from costimulators on the DC can differentiate into T-regulatory cells (Tregs) [7]. Tregs suppress activation of lymphocytes and are important for the maintenance of immunological tolerance, which is the immune system's ability to remain unresponsive toward antigens that are not harmful [10].

The cell-mediated immune response is provided by the lineage of CD8+ cytotoxic T cells (CTLs), as well as NK cells and macrophages. CTLs and NK cells kill pathogens by secreting cytotoxic granules that induce apoptosis of the target cell. Macrophages are phagocytotic, meaning they kill pathogens by ingesting them. Like CD4+ TH cells, CTLs must also be presented an antigen through an MHC molecule. The MHC needed to activate CD8+ CTLs is the major histocompatibility complex class I molecule (MHC I) [7]. While MHC II only is expressed by APCs, MHC I is expressed by all nucleated cells [8].

1.3 Human Immunodeficiencies

Malfunction of cells constituting the immune system can lead to diseases known as immunodeficiencies. Immunodeficiency refers to the compromise of the immune system, making the individual more prone to infection and disease, such as cancer, allergy, and autoimmunity disorders. Immunodeficiencies are categorized into congenital (primary) immunodeficiency and acquired (secondary) immunodeficiency. Congenital immunodeficiencies are caused by abnormalities in genes involved in the development or proper function of various immune cells and are usually revealed during infancy or early childhood. Acquired immunodeficiencies, on the other hand, occur later in life and are most often caused by pathogen infection, such as the HIV virus. Acquired immunodeficiencies can also be a result of disease progressions, such as cancer pathogenesis, or therapy against cancer, e.g. chemotherapy [7].

1.3.1 SCID

Congenital disorders affecting both humoral and cell-mediated immunity are classified as SCID. These are monogenic immune diseases and result as the consequence of impeded T cell development, which in some cases is accompanied by defective B cell maturation as well [7]. For SCID not to be fatal, patients with this disorder must be treated immediately to reconstitute their immune system. An opportunistic infection that would only cause mild symptoms in healthy people would be life-threatening in SCID patients [7, 11]. Many viruses have the potential to cause serious diseases in SCID patients, for instance, Chickenpox (Varicella). For people with fully functional immune systems, a chicken pox infection affects the skin and mucous membranes only. However, for SCID patients, this virus can affect the lungs, liver, and brain (Abbas et al., 2018). If SCID is not discovered and diagnosed early in life, patients often die by the age of 2. SCID can be treated by HSCT or by gene therapy strategies [11].

1.3.2 ADA2

Adenosine deaminase type 2 (ADA2) has a critical function in adaptive immune system development. ADA2 acts as a protein helping in the degradation of extracellular adenosine but also has a role as a growth factor [12]. Deficiency in *ADA2* (DADA2) is an autosomal recessive genetic disease, and the disease results from loss of function by several mutations spanning across the *ADA2* locus. Patients with DADA2 have systemic inflammation and vasculitis but other symptoms are common too. ADA has two isoforms of adenosine deaminase (ADA1 and ADA2) whereas DADA2 can cause SCID [13]. There are few available treatments for DADA2 whereas HSCT has high potential [13]. DADA2 was described for the first time in 2014 and there is still a lot to be learned about this disease [12].

1.4 Hematopoietic Stem Cell Transplantation

Patients of high-risk hematological malignancies and genetic disorders of the hematopoietic and immune system can be subjected to allogenic HSCT, meaning transplantation of HSC that is not genetically identical to the recipient [2, 14]. The goal of HSCT is to replace the patient's hematopoietic and immune system with that of a healthy donor by engraftment of normal HSC and progenitor cells, often collected from the donor's bone marrow. Allograft rejection due to lacking histocompatibility between the donor and recipients MHC molecules is a major issue in HSCT [2]. Alternatively, HSCT can be done autologously, which means HSCs are extracted from and reinfused into the patient. Autologous HSCT often involves genetic engineering of the patient's HSCs to regenerate the immune system [15].

The human MHC loci are located on the short arm of chromosome 6 and encode the HLA molecules (human leukocyte antigen). Human MHC class II molecules include HLA-A, -B and -C. These are the molecules needed for TH cell activation. The CTL binding MHC class I molecules found in humans are HLA-DR, -DQ, and -DP [16]. The genes of the HLA loci are highly polymorphic and can contain up to 699 alleles per locus, which is the case for HLA-B [17]. Such extensive polymorphism makes for high diversity in the HLA expression profile between species and individuals, which is essential to effectively combat a wide range of pathogens and infections but has proved to be unbeneficial in transplantation medicine. In allograft transplantation, donor

HLA is presented as a foreign antigen to the recipient of the graft, of which the immune system will elicit a response. In this response, the APCs of the recipient initiate the process of graft rejection, which is comparable to the normal immune response elicited towards a pathogen. This is called indirect allorecognition. It is also possible for the immune cells of the graft to elicit a response against the cells of the recipient and is called direct allorecognition [18].

Due to the low tolerance of genetic differences in HLA, it is critical that the HLA is matched between the HSC donor and recipient [19]. HLA mismatch can cause graft-versus-host-disease (GVHD) and in the worst case, death [17]. GVHD is a condition that occurs in transplanted patients and is the immune reaction of donor T cells towards antigens of the recipient and can be both chronic or acute. Acute GVHD most frequently affects the skin, as patients often develop rashes. The gastrointestinal tract and liver are often also affected. Patients can experience liver dysfunction, vomiting, abdominal pain, and severe diarrhea leading to a breach of mucosal membranes and bleeding. In cases of severe acute GVHD is often lethal. Chronic GVHD is the largest cause of death in HSCT patients and often emerges in elderly patients or those who have previously been affected with acute GVHD [20]. The frequency of acute GVHD directly correlates with the degree of HLA mismatch, however, the condition can develop in both matched and unmatched HLA donors, and it is proposed that about 40% of HSCT patients who receive grafts with identical HLA experience GVHD. Other than differences in the MHC loci, GVHD arises due to polymorphisms in other genres as well, such as cytokine genes or the NOD2/CARD15 gene involved in innate immune responses [16, 20]. Finding a perfectly matched HLA is challenging and not necessarily sufficient for successful engraftment. Current HSCT research is highly focused on overcoming this obstacle by identifying permissible HLA mismatches to improve the success of engraftment from unrelated donors and decrease the T cell alloreactivity [17].

1.4.1 Usage of Humanized Mice in HSCT Research

Although life-threatening, the use of the SCID mice in research has been beneficial to human biology and medicine. Their lack of ability to elicit an adaptive immune response towards foreign antigens makes this mouse model suitable for human engraftment studies [21]

In 1988, the SCID-C.B-17 mouse strain were implanted with T-cell enriched human fetal thymus tissue and HSC enriched human fetal liver cells, leading to the construction of the first mouse strain (SCID-hu) with functional T cells of the human immune system [22, 23]. Further investigation on the SCID-hu strain revealed that the strain was highly susceptible to HIV-1 [23]. This mice strain and others have been created and still are an important part in the understanding of HIV gene function, replication, cellular tropism, pathogenesis, treatment, and hopefully a cure for the disease [24].

An example of a SCID mouse strain is the NOD.Cg-*Prkd*^{scid}*Il2rg*^{tm1Wjl}/SzJ, often referred to as NOD SCID Gamma (NSG™). This strain of mice carries two mutations. The first is SCID mutation in the repair complex protein in *Prkdc gene,* which restricts B and T cell development. The other one is a complete null allele of the IL2 receptor, which prevents cytokine signals through multiple immunity-related receptors meaning deficiency in natural killer cells [25].

Humans and mice are both mammals and their organs are identical in shape, structure, and physiology [26]. For a long time, there was a need for a small animal model in preclinical research to study human immunity and other complex biological processes. In vitro and ex vivo experiments alone are not capable of carrying out these complex biological systems. The mouse model has gradually improved, and the use of humanized mice in preclinical research has grown. Humanized mice refer to mice that have been subjected to transplantation of human cells, tissue, or transgenic expression of human molecules such as HLA [21].

1.5 Animal Models

The mouse is the most common choice of an animal model when investigating human physiology and biology [26]. Several animal models can be chosen for different research purposes. When an experiment is designed to use animals, selecting a model that fits the experiment is important. Rabbits, usually *Oryctolagus cuniculus,* have been used as research animals in Europe since 1850 and have similar anatomy to other mammalians. It is easy to spot the central ear artery and marginal era veins in the big ears, which can be used for intravenous access and blood sampling. They are often used as a model of a human pregnancy and in immunology in the production of polyclonal

antibodies because their blood volume is more extensive than rodents. They can also be used in atherosclerosis, osteoporosis, and ocular research [26].

Rats have undergone testing since 1828, and *Rattus norvegicus* is the most used in research. They have been used in several research fields, from space exploration to basic research like nutrition. Rats are used primarily for the development of new drugs [26]. Moreover, it is a great model used in addiction-like behavior studies or studying biochemical responses from epilepsy in the rat brain [27] [28]. Mice and rats share some common advantages as animal models. From the economic view, rodents are small, requiring small space or resources to maintain [29]. The gestation time is approximately 19-21 days for mice and 21-23 days for rats, with a litter size of 9-12 for both [26]. In addition, they have rapid development, reach sexual maturity by five to six weeks, and have a short life span. Therefore, it is possible to generate many rodents in a relatively short time [29].

1.5.1 Drug Testing Using Animal Models

In 1937 a pharmaceutical company in the USA developed a drug, and they put it on the market. The company prepared sulfanilamide with diethylene glycol (DEG), and the raspberry flavor put in the drug was dissolved in it. The company did not know that DEG was poisonous to humans, and they did not do any testing on animals before it was released. The consequence of this was that over a hundred people were poisoned and died. Because of this incident, a new law was put in demanding federal food, drug, and cosmetics to test their products on animals before being bought in shops [30]. Another tragedy happened in the 1950s with a drug. Thalidomide was developed as a sedative drug and often used by women who struggled with morning sickness. The drug had been on the market for two years before the first indication of fetal deformities when a child was born with phocomelia in all limbs. The drug was tested on mice, rats, guinea pigs, and rabbits for 30 days at high concentrations without any observed abnormalities. However, one of the problems with this experimental design was that they did not test them on pregnant animals [31]. In 1962 Thalidomide was tested more thoroughly on rabbits with 150 mg per kg from day 8 to 16 in pregnancy. The dose the rabbits got was higher than a human would take. However, the deformities of the newborn rabbits were like ones that could be seen in humans [32].

1.5.2 Use of Animals in Science

The use of animals in science is an ongoing debate. Animal models have played an essential role in helping to answer a variety of scientific questions, especially in the assessment of novel vaccines or therapies [33]. When human and mouse genomes were compared in early 2000, it was found that over 90% of the genomes could be partitioned into corresponding regions of conserved synteny [34]. Synteny in the dictionary would be described as “same ribbon” but is interpreted as “on the same chromosome” [35]. In addition, there are vast commonalities in biology. Human diseases often affect other animals, and the mechanism is very the same. For instance, the veterinary drug is so similar in action to the one used to treat humans (Barré-Sinoussi and Montagutelli, 2015). Banting and MacLeod received a Nobel prize in 1923 for treating Type I diabetes and established testing on a diabetic dog. Surgical techniques have been developed and improved using pigs as models before being applied to humans (Barré-Sinoussi and Montagutelli, 2015). Essential vaccines save millions of lives every year, and development is successfully completed by using animal models. For example, when BioNTech-Pfizer COVID-19 vaccines were under development, testing was performed on female BALB/c mice (8-12 weeks old) and Rhesus macaques (2-4 years old) [36]. Nevertheless, in vivo experimentation and testing requires strict legislation and researchers must follow the national and local authority's laws and guidelines together with their own best practice.

1.5.3 Three R´s

One thing which is often debated about using animal models for scientific purposes is the welfare and protection of the animals. The European directive 2010/63/EU has set the framework for handling and treating animals used for scientific purposes [37].The regulation is based on three fundamental principles known as the 3Rs rule:

I. Replace: Animals shall not be used whenever other options non-animal-based are available with similar relevance and reliability.
II. Reduce: The number of animals to be used shall be adjusted to the minimum to conclude.
III. Refinement: Optimize the methods to minimize the potential stress, pain, and distress the animals would be exposed to.

To be able to work with animals in research in Norway, it is required to take a mandatory course according to Norwegian regulations on Animal experiments (FOR-2015-06-18-761). This course is based on Articles 23 and 24 of the EU Directive 2010/63/EU. The certificate will be practical and theoretical with function categories A, B, and D. This certificate is valid in other parts of the European Union. When a project is being designed, it is essential to implement these three R´s to make the best possible decision/conditions for the animals. Another important thing to look at is the cost-benefit analysis to conclude how much harm it will cause to the animal and how much knowledge the experiment will generate.

1.6 Genome editing

Before genome editing tools were available there were other options to induce mutations in the genome of various organisms. This was mainly done in plants by cross-pollinating or cross-breeding [38]. In 1970, the first recorded gene-targeted alteration was achieved in yeast. Ten years later, in 1980, this was also done in mice [39].

Genome editing has the potential to edit cells by inserting, removing, or editing DNA or RNA [40]. Targeted nuclease is the foundation of this field since it breaks the chromosomal DNA and can target and alter any DNA sequence in all cells. After a double-strand break (DSB), the cellular DNA repair machinery has two main options. One is to join the cleaved ends together by the mechanism called non-homologous end-joining (NHEJ) (Figure 2A). NHEJ is a quick fix and is likely to induce insertions and/or deletions in the DNA, called indels [40]. The second is the homology-Direct DNA repair (HDR) pathway, which uses a donor template. This template can be engineered to contain the desired mutation (Figure 2B). Such templates include the single strand oligodeoxynucleotide (ssODN), which is preferable for small insertions or deletions and can only install short changes in DNA [41]. Another template is the double-stranded oligodeoxynucleotides (dsODN), which is used to insert larger sequences [42]. ssODN and dsODN can be delivered to the cell by electroporation, which involved electric shocking of the cell [43]. An alternative to template delivery to cells by electroporation, is genomic integration through the adeno-associated virus (AAV). This is a viral vector donor with a cargo size of about 4.5kBp, used to insert large sequences. After the vector has been transported into the nucleus, the viral ssDNA is uncoated and

integrated into the host genome by HDR. AAV can be delivered directly to the living organism, contrary to the dsDNA/ssODNs strategies but is more difficult to design, manufacture and pose risks to the organism. [44]

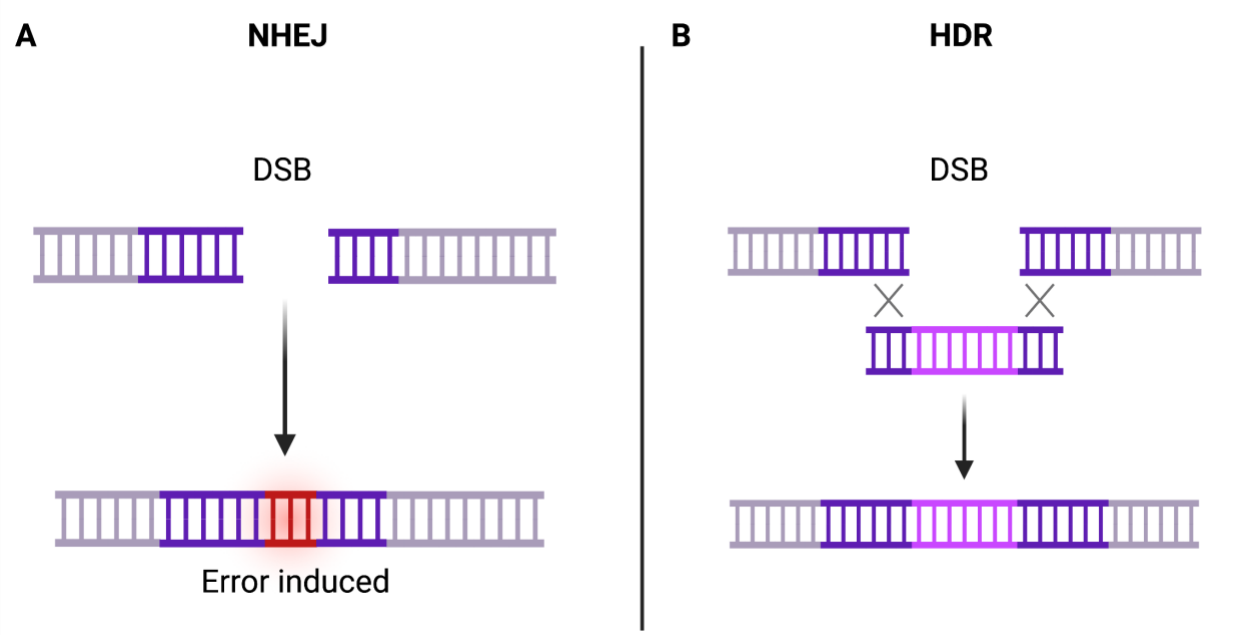

Figure 2. Repair pathways after double-strand break (DSB) of the DNA. A) *Non-homologous end joining (NHEJ) is the canonical and fastest repair pathway. This pathway is error-prone and often results in insertions of random nucleotides (red base pair).* ***B)*** *HDR is a slow but precise repair pathway that uses a template sequence to copy in order to join the ends. By designing the template sequence, HDR makes it possible to insert long coding sequences into the genome. Created in BioRender.com*

In 1985 a symmetric dimer with a palindromic sequence was discovered to recognize DNA. This discovery led to a new technique in genome editing called Zinc finger nuclease (ZFN) (Figure 3A) [45]. ZFN was engineered by fusing the zinc-finger DNA-binding domains of zinc-finger proteins with the cleavage domain of FokI and allows editing of an abundant number of target sites with relatively short sequences (9-18nt). For ZNF to cleave DNA at the target site, two zinc finger proteins must bind close to the spacer on each strand, which allows FokI endonuclease to form a functional dimer (Zhang et al., 2019). ZFN proved to be only a small contribution to the genome-editing field, as the DNA binding domain was hard to design for precise and effective cutting at the target site. ZFN design is time demanding and complex, often resulting in an off-target editing [46, 47].

In 2011, a new technique was adapted from a naturally occurring gene regulation system in *Xanthomonas* bacteria. It was named Transcription activator-like effector nuclease (TALEN) (Figure 3B). TALENs contain a DNA-binding domain with a highly conserved 33-35aa repeat sequence, each recognizing one base pair [40]. The main difference between ZFN and TALENs is the way of recognizing DNA. TALEN is designed to recognize single nucleotides, while ZFN recognizes triplets of nucleotides. There are several benefits with TALEN compared to ZNF. TALEN is easier to design and causes fewer off-target effects. However, TALEN also has some disadvantages, e.g., larger size, which makes it difficult to deliver and express in cells and host organisms [47].

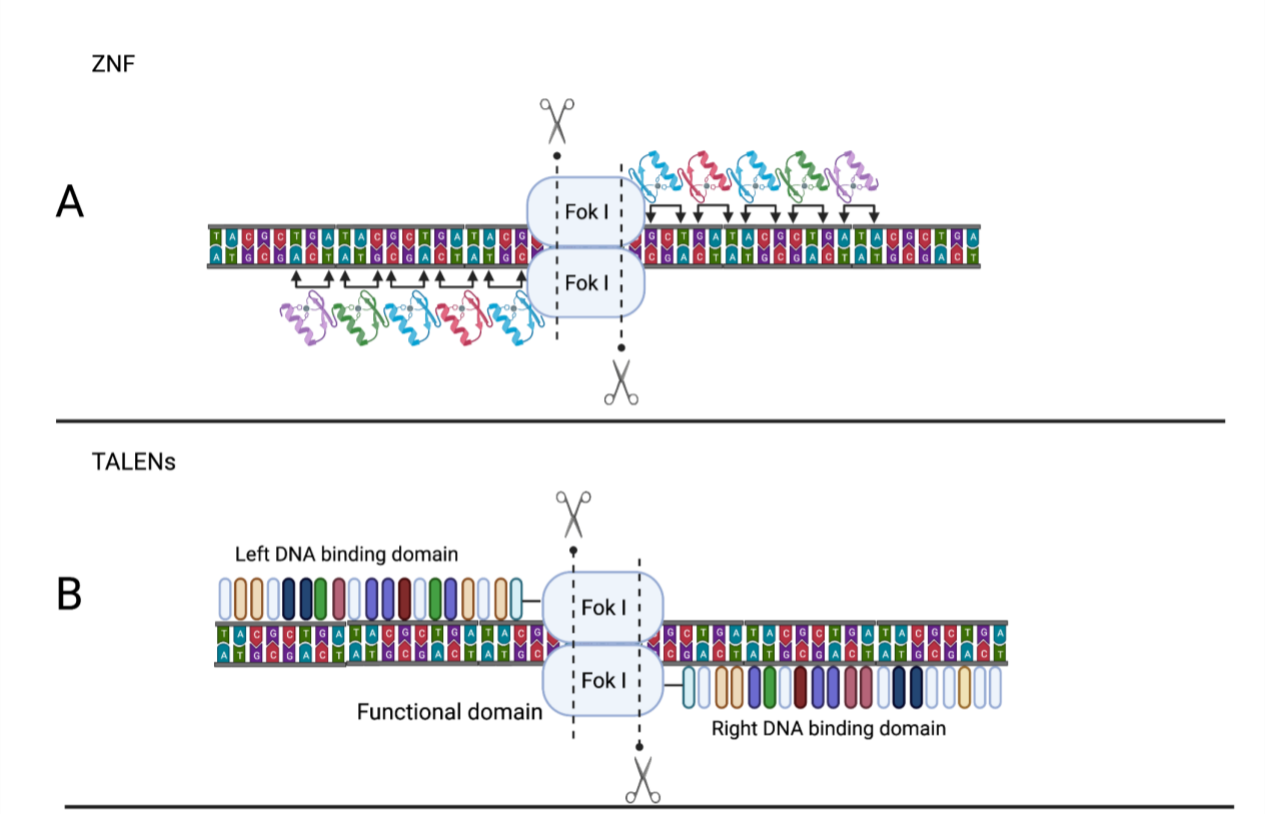

Figure 3. Comparison of the ZNF and TALENs genome editing tools

A) illustration of ZNF symmetric dimer with a palindromic sequence. The most common DNA-binding motif is the Cys_2-His_2 zinc-finger domain. One zinc finger consists of approximately 30 amino acids (aa) in a beta-beta-alpha configuration. The number of Cys2-His2 zinc-finger domains vary from 3-to 6, where each of them recognizes three nucleotides (Gaj et al., 2013) (Zhang et al., 2019). B) TALENs with single nucleotide recognition. fused a catalytic domain FokI endonuclease with a DNA-binding domain derived from transcription activator-like effectors (TALEs). Created in BioRender.com

Zinc-finger nuclease (ZFNs), Transcription activator-like effector nuclease (TALENs) are famous tools in genomic engineering and are still in use today. However, when Clustered Regularly Interspaced Short Palindromic Repeat (CRISPR) was invented, the potential it brought changed the whole gene editing field and the entire perception of the biology [48].

1.6.1 CRISPR/Cas9

The principle of CRISPR was discovered in 1993. However, nearly two decades went by before CRISPR really took off. In 2012, the team of Jennifer Doudna and Emmanuelle Charpentier showed how CRISPR made precise targeted cuts, thus portraying its potential in the gene-editing field [49]. Eight years later, Doudna and Charpentier won the Nobel prize in chemistry for the development of the CRISPR-Cas9 enzyme (Figure 4) derived from *Streptococcus pyogens* (SpCas9). SpCas9 is the most used nuclease in gene editing and is a defense mechanism against foreign DNA facilitated through RNA-guide cleavage [50]. CRISPR-Cas systems are divided into classes 1 and 2 with several subtypes. The class 1 CRISPR-Cas system has multi-Cas effector molecules. These complexes are responsible for DNA recognition and crRNA binding. Class 2 CRISPR-Cas is simpler, with just a single Cas protein responsible for binding and cleaving DNA molecules. Class 2 systems are capable of targeting both DNA and RNA. Cas9 is a member of class 2 CRISPR-Cas system, which also carries the assisting proteins of Cas1 and Cas2. It targets DNA and requires tracrRNA for function [51].

The first article to show genome engineering using the CRISPR-Cas9 system to edit eukaryotic cells was published in 2013 [52]. To cut DNA, the Cas9 protein needs to be assembled with a guide-RNA (gRNA) in the form of crRNA and tracrRNA or fused into a single-guide-RNA (sgRNA) [53]. This gRNA is 20nt long and complementary to a 20bp DNA sequence to which the gRNA binds. Comparing it to other tools, base to base recognition is precise and the gRNA can easily be changed to any wanted base [50].

It is essential to design the gRNA to match the DNA adjacent to the protospacer adjacent motif (PAM) since PAM work as a switch to trigger Cas9 to induce DSB in the complementary strand and non-complementary strand by its nuclease domains HNH and RuvC, respectively [54]. DSB

is a severe lesion to multicellular organisms and results in induced DNA repair by endogenous cellular pathways, which can introduce alterations to the DNA sequence, including indel changes [50].

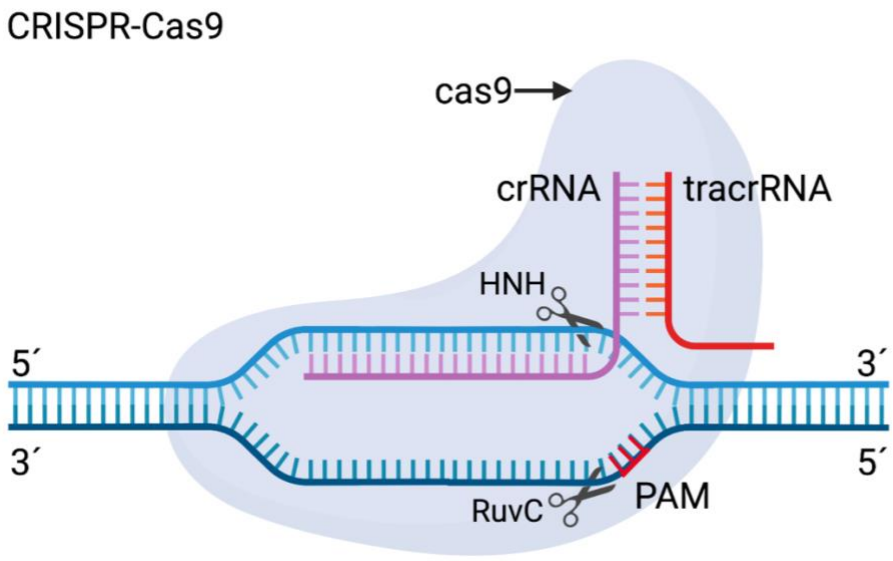

Figure 4: The CRISPR-Cas9 genome editing tool. *CRISPR-Cas9 binding to a target DNA sequence (blue) with gRNA (crRNA (purple) and tracrRNA (red)) induces double-strand breaks in the complementary strand (lighter blue) by HNH and in the non-complementary strands (darker blue) 3 base-pairs upstream of PAM motif by RuvC. Created in BioRender.com*

1.6.2 Optimization of gene editing tools

One of the most dangerous events that can occur inside the cell is a DSB of the DNA. To avoid this, the cells are protected by various and complex DNA repair pathways interconnected with each other [55]. Thanks to this balanced and precisely tinkered relationship, the cells can maintain the integrity of their genome. Optimization of CRISPR for precise editing is focused to limit the NHEJ pathway and increase HDR events. NHEJ is the dominant repair solution and is not limited to a cell cycle phase. On the other hand, the template based HDR pathway is limited to the S/G2 phase of the cell cycle [56]. By promoting entry into the S/G2, blocking the NHEJ pathway, and inhibiting 53BP1, which accumulates at DBS and promotes NHEJ, the cell is forced to repair the

DBS by HDR (Figure 5) [56]. Other tools based on CRISPR/Cas9 technology have emerged recently, for instance, base editors and prime editors. These methods skip the introduction of DSB and are safer and more suitable for precise gene correction of monogenic diseases. However, optimization steps are still required before the translational process toward the clinical application [57, 58].

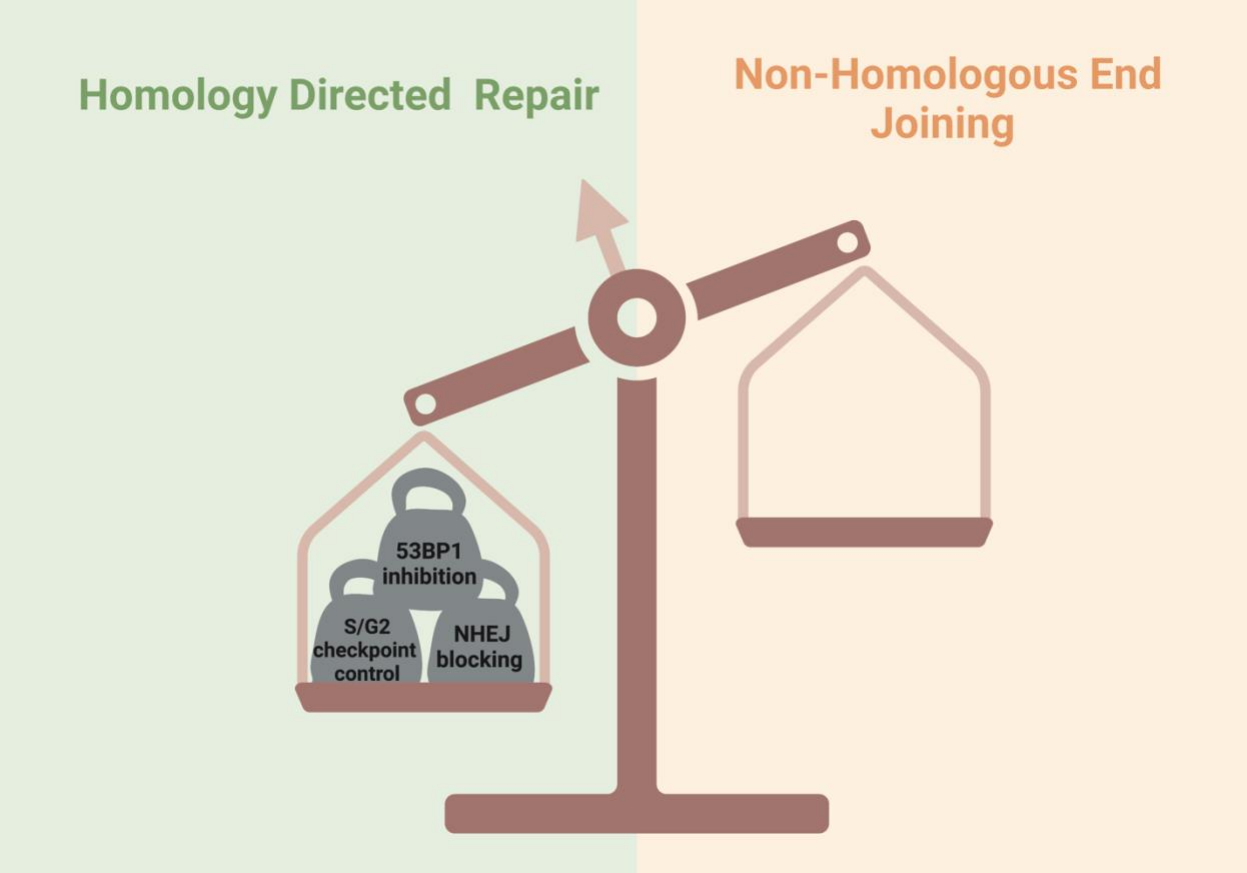

Figure 5. Hypothetical overview of tipping the balance of DSB editing outcomes to favor HDR. *Inhibition of 53BP1, NHEJ blocking, and S/G2 checkpoint control (grey weights) tips the hypothetical scale to favor the HDR pathway which allows for the integration of the desired template. Created in BioRender.com*

1.7 Aims of the thesis

The aim of this master thesis is divided into an *in vivo* and *in vitro* part. The *in vivo* study using a mouse model was split into two parts. The first part is mastering the general *in vivo* techniques such as getting familiar with mouse behavior, handling the mice, performing ear marking, euthanasia, mouse dissection, and organ collection. The second part of the *in vivo* experiment included an evaluation of human engraftment in irradiated mice injected with edited or unedited HSPCs.

In the *in vitro* part, the aim is the optimization of gene editing techniques using the CRISPR-Cas9 system and healthy donor fibroblasts. The goal is to increase the number of HDR events compared to NHEJ by promoting cellular conditions favoring the HDR repair pathway, which includes blocking the NHEJ repair pathway. By increasing the HDR events, we would like to consequently enhance the precise integration of the repair template using CRISPR-Cas9.

The long-term goal of the *in vivo* and *in vitro* study is to optimize gene therapy strategy employing CRISPR-Cas9 and short repair template and apply our knowledge to the clinical treatment of childhood monogenic immune diseases.

2. Materiel and methods

2.1 Bought material

RNP mix

- ADA2 sgRNA #3 (IDT)
- ADA2 repair template (ssODN) forward (IDT)

ddPCR

- ADA2 ddPCR primer forward (IDT)
- ADA2 ddPCR primer reverse (IDT)
- ADA2 ddPCR FAM (IDT)
- ADA2 ddPCR NHEJ probe (IDT)
- ADA2 ddPCR HDR probe (IDT)
-

Plasmids

- Ad5 E4ORF6/7 (Synthesized as a gene fragment from GeneArt, Thermofisher)
- CYREN (Synthesized as a gene fragment from GeneArt, Thermofisher)
- Cry1 variants (Synthesized as a gene fragment from GeneArt, Thermofisher)
- GSE56 (Synthesized as a gene fragment from GeneArt, Thermofisher)
- i53 (Addgene)
- EGFP (Addgene)

Fluorochromes

- CD45 Pacific Blue (BioLegend)
- Aqua dead Viability (ThermoFisher scientific)
- HLA-ABC Alexa Flour 700 (BioLegend)
- mTER119 PE-Cynine5 (BioLegend)
- CD45.1 PE-Cynine7 (BioLegend)
- CD45 Brilliant violet 711 (BioLegend)
- CD45.1 PE (BioLegend)

2.2 *in vivo* Engraftment Experiment

2.2.1 Mice Housing Conditions

All the mice were handled according to national laws and regulations of Norway and Mattilsynet (FOTS ID 24187). The mice were kept in a minimal disease unit (MDU) in the animal facility at Rikshospitalet. Mice were kept in an individual ventilated GM500 Cage (Tecniplast Group) in a DMG rack. 48 female NOD.Cg-*Prkdc*^{scid} *Il2rg*^{tm1Wjl}/SzJ 6 weeks old mice were purchased from The Jackson Laboratory (USA). Mice were randomly divided into five treatment groups consisting of nine mice and a different control group with three mice. Each treatment group had two dedicated cages into which mice were housed accordingly to the animal facility rules. Identification of each mouse was made by punching holes (marking 1#-5#) in the ear in each cage. The different treatment groups received unedited or CRISPR-Cas9 *ADA2*-edited hematopoietic stem and progenitor cells (HSCPs). Additionally, the HSCPs in treatment groups were kept *in vitro* culture for different time (Table 1). The cages were changed twice a week for the first four weeks after irradiation and then changed once a week until reaching the humane endpoint of 12 weeks. The mice were kept in 12h:12h of light and dark regime provided with unlimited food and water and proper enrichment (chewing sticks, houses, cotton wool cones, and building material for the nests). The mice were provided with acidic water to prevent bacterial infection and dietary gels to provide fast revitalization after irradiation during the experimental window. The control group did not receive acidic water or recovery gel.

Table 1: Setup of treatment groups

Treatment group	Edited/unedited	Days in culture	Source of HSPCs	Injection volume	Mice
Control	PBS injection only	n/a	n/a	n/a	3
Group 1A	Unedited HSPCs injected	4	AllCells	200 000 cells/200ul	9
Group 2A	Edited HSPCs injected	5	AllCells	200 000 cells/200ul	9
Group 2B	Edited HSPCs injected	4	AllCells	200 000 cells/200ul	9
Group 3A	Unedited HSPCs injected	4	Local donor	200 000 cells/200ul	9
Group 3B	Edited HSPCs injected	4	Local donor	200 000 cells/200ul	9

2.2.2 Irradiation and HSPC Injection into Mice

All mice were weighted to establish base weight before the irradiation procedure. Mice were transported from the animal facility in sealed GM500 cages to the X-ray machine situated at the Immunology department in Rikshospitalet **(**OUS). Each mice cage was irradiated with two doses consisting of 1.25 Gy, 2.5 Gy in total, with 4-hour break between each dose. The mice in the control group were not irradiated at all. Within a window of 24hrs post-irradiation, the mice were prepared for injection of HSCPs (Figure 6). The GM500 cages were kept on a heating mat and were simultaneously warmed by an infrared heating lamp. The tail vein became easily visible and accessible after 10 minutes. The mice were restrained in a tube and the injection was performed using intravenous access via the tail vein. The mice were injected with either stem cell solution (200 000 cells/200ul) or sterile PBS solution (200µl). Injection of HSCPs in the tail vein was performed by a supervisor. After injection, the mice were observed for a few minutes to ensure they recovered from the warming and injection events. Afterward, the mice were followed up daily for four weeks to observe any signs of post-irradiation sickness. The mice were sacrificed by cervical dislocation at the humane endpoint 12 weeks after injection. All mice that lost more than 15% of the base weight and showed signs of severe pain and /or distress were sacrificed by cervical dislocation.

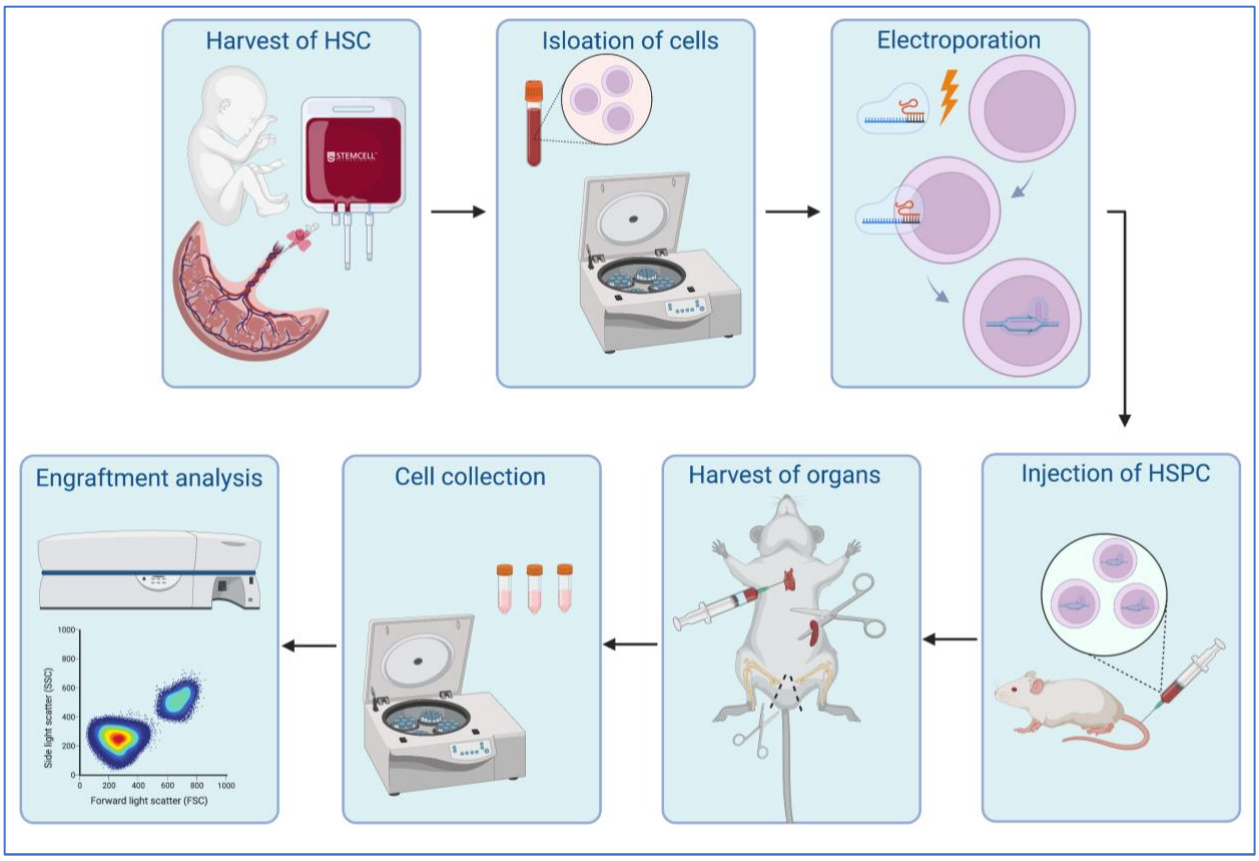

Figure 6: Pipeline of the mice experiment from the collection of HSCs to analyze the human engraftment. *Cord blood enriched with HSCs was harvested from the human placenta. HSPCs were isolated by centrifugation. HSPCs were electroporated and edited by CRISPR-Cas9. Edited HSPCs were injected into mice. Organs (i.e. bone marrow, spleen, and peripheral blood) were harvested from euthanized mice. Cells of the different organs were collected. Human engraftment was analyzed by flow cytometry. Created in BioRender.com*

2.2.3 Termination and collection of mice organs

One at a time, the mice were transported from the cage into a chamber filled with isoflurane to anesthetize the animal. After 2 minutes with isoflurane, the mouse was in a deep sleep and was euthanized by cervical dislocation with a metal plate to prevent further damage to adjacent organs and blood loss. After cervical dislocation, the mouse was pinned down to cardboard with needles. The mouse was sprayed with ethanol so the fur would lay down, and it was easier to see the skin. Next, the opening cut was performed with scissors and a tweezer to access the heart without much delay (Figure 7A). The mouse was sprayed with ethanol so the fur would lay down, and it was easier to see the skin. The skin above the tail was lifted with a tweezer and cut with a scissor up to the throat so the heart would be easily accessible (Figure 7B). The skin was pulled out to each side

and pinned down. A syringe and collection tube was coated with anti-coagulating substant (50mM EDTA). The needle was inserted into the heart in approx. 45 degrees. The plunger was pulled out while the syringe was making a pumping motion and transported into an Eppendorf tube with 10ul of anti-coagulating substant. The blood collection was repeated to ensure enough volume of peripheral blood was collected and was kept at room temperature. Further, the tweezer was used to find the spleen under the intestines on the left-hand side of the mouse. The spleen was cut out, trimmed, and transported into a different Eppendorf tube filled with cultivation media (RPMI or DMEM) and was kept on ice. For bone collection, both femurs and tibias were collected from each leg (Figures 7C and D). The entire leg was cut above the femur joint and kept intact for the best result. Fur, skin, muscles, and connective tissues were removed, trimmed, and placed into a 50 ml falcon tube prefilled with 1x PBS and kept on ice.

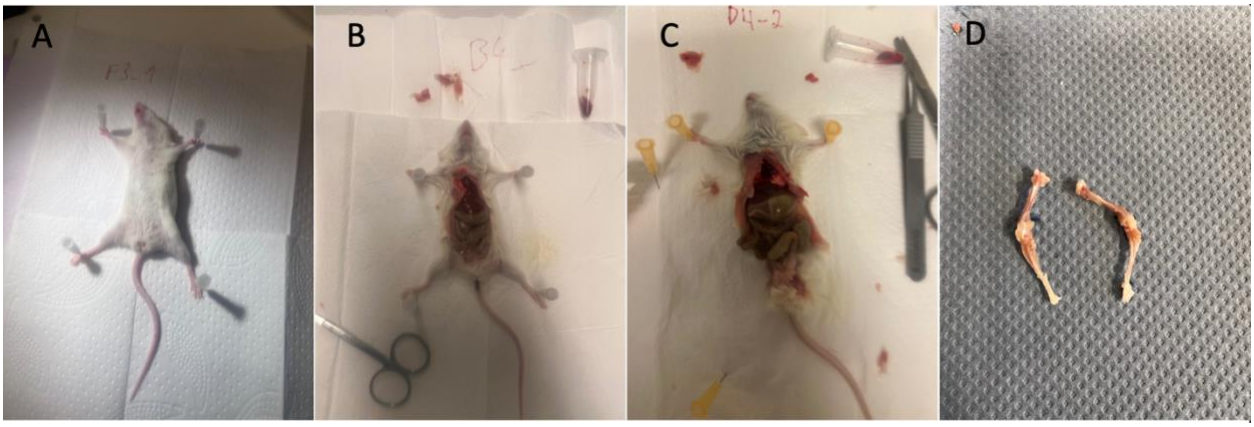

Figure 7. Dissection of mouse for blood, spleen, and bones (femur, tibia) collection.

A) After cervical dislocation the mouse was pinned down. B) The mouse was cut open and blood was collected, as can be seen in the Eppendorf tube in the top right. C) and D) Both legs were cut off and cleaned to the bone before being put in 1x PBS on ice. Pictures (A-C) were taken through a plastic bag which made them blurry.

2.2.4 Extraction of Cells from Bone Marrow

For bone marrow extraction, the centrifugation method from Heib et al., 2021 [59] was used. First, a clean 0.5ml Eppendorf tube was poked, and a small hole was created with a syringe needle (18G). Next, a new 1.5ml Eppendorf tube was filled with 100ul of 1xPBS, and the small 0.5ml Eppendorf tube with a hole was put inside the 1.5ml Eppendorf tube. Bones from a 50 ml falcon tube were taken out, and the femur and tibia were separated by cutting the knee joint's back. A small piece

of the head of the tibia was cut off, and the same from the bottom of the femur. Next, the femur and tibia were placed into the 0.5 mL Eppendorf tube with the open end downwards and centrifuged at 2500g for 1 min (Figures 8A and B). Bones that had extracted bone marrow would appear white and were discarded (Figure 8C). If necessary, this step was repeated.

1 ml of 1x PBS was added and resuspended by pipetting ten times. A new mesh filter was placed on top of a new falcon tube. The filter was washed with 1 ml of 1xPBS, and the cell mixture was loaded onto the filter. A syringe plunger was applied and pressed the cells gently through the filter. Before discarding it, the filter was washed once more with 1 ml of 1x PBS. A new 40 um filter was placed onto the new falcon tube, and the same procedure was repeated with the new filter. The filter was discarded, and the cells were centrifuged at 300g for 5 min. The supernatant was carefully removed, and the cells were resuspended slowly in 5 ml of 1x RBC lysis buffer before placing them on ice for 3 min. 45 ml of ice-cold 1x PBS was filled into the tube and spun down. The supernatant was discarded, and the cells were resuspended in 20 mL of 1x PBS before counting them and subjecting them to flow cytometry.

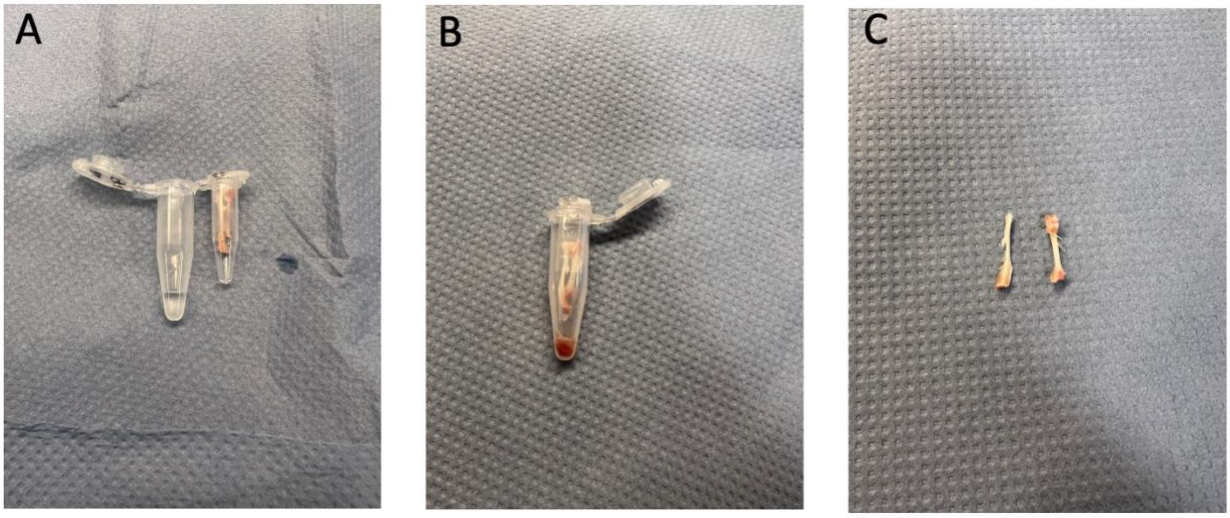

Figure X. Extraction of bone marrow cells by centrifugation. *A) The femur and tibia were split at the knee joint and place into a small Eppendorf tube. Bigger Eppendorf tube was filled with 100µL of 1xPBS. B) Bone marrow was extracted after centrifugation. C) Successful extraction/collection of bone marrow from femur and tibia would made the bones become white. The leftover red part was untrimmed muscle tissue.*

2.2.5 Extraction of cells from the spleen

A new 70 µm mesh filter was placed into a 50 ml falcon tube, and the spleen was transported from the Eppendorf tube to the filter. Tweezer was necessary to hold the spleen and cut small fragments with a scissor onto the mesh filter. RPMI or DMEM media without antibiotics was added to the filter so the spleen would not dry out. The spleen tissue was pressed gently with the syringe's plunger (5ml) until it got pale, and the cells were collected by washing the 70 µm filter with 1 mL of 1x PBS. 30 mL of 1x PBS was added and the cells were spun down at 2000 RPM at +4° for 10 min. Next, the supernatant was removed, and 5 mL of lysis buffer got added and incubated for 3 minutes on ice. 40 mL of 1x PBS was added to the falcon tube and spun again. The supernatant was discarded and resuspended in 5 mL of 1x PBS. The cells were filtered through a 40 µm mesh filter to remove clumps and other debris. The cells were counted and stored on ice until further flow cytometry analysis.

2.2.6 Extraction of the cells from peripheral blood.

For peripheral blood cell isolation, we followed the protocol by Bak et al., 2018 [60]. A new 1.5 mL Eppendorf tube with 500 µL of PBS with 2% dextran was added to the blood and mixed well. The tubes were incubated at 37°C for 30 minutes to allow red blood cells sedimentation. After incubation, the leukocyte-rich plasma layer was carefully transferred into a new Eppendorf tube without disturbing the sediment of the red blood cell layer. 500 µL of ice-cold FACS staining buffer was added into the new tube and centrifuged at 300g for 5 minutes at 4°C. The supernatant was aspirated, and the cells were resuspended in 500 µL of red blood cell lysis buffer and incubated for 3 minutes on ice. 5 mL of FACS staining buffer was added to the tube, and the samples were spun down at 300g for 5 minutes at room temperature. The supernatant was removed, and the cell pellet was resuspended in 100 µL of 1x PBS. The cells were kept on ice.

2.2.7 Flow cytometry analysis of human engraftment

The cells from bone marrow, spleen, and peripheral blood were resuspended at 1 x 10^7 cells/mL in 1x PBS, and it was taken an aliquot of 1 x 10^6 cells (100µL) into separate wells of a 96-well plate. Stained and unstained conditions were included for setting the gates later. Before the cells were stained, they were washed in 1xPBS to remove any debris from the RBC lysis buffer. 5 µL of Human Monocyte Trustain and 5 µL of Human Trustain were added per 100µl cell solution and

were incubated for 20 min on ice in the dark. Next, 1uL of Aqua dead viability stain was added and incubated for 30 min on ice in the dark. The cells were spun down at 500g for 5 minutes and the supernatant was removed. FACS staining buffer was made by adding 2% FBS to 1x PBS before the cells were resuspended in 200ul of FACS staining buffer and spun down at 500g for 5 minutes. This step was repeated once more. After the last wash, the flow cytometry-specific master mixes were prepared and added to the cells.

For flow cytometry panel 1, the following antibodies were used: 5µL of HLA-ABC-Alexa-Flour 700, 5µL of hCD45-Pacific Blue, 1µL of mCD45.1-PE-Cy7, and 1µL of TER119-PE-Cy5.
For flow cytometry panel 2, the following antibodies were used: add 5µL of hCD45-PE and 1µL of mCD45.1-BV711. After adding the flow-cytometry-specific master mixes to the cell solutions, the cells were kept on ice in the dark for 30 minutes. Next, 100 µL of FACS staining buffer was added to the cell mixture and centrifuged at 500g for 5 min at room temperature. The supernatant was discarded, and the cells were resuspended in 200 µL of FACS staining buffer. The cells were centrifuged at 500g for 5 minutes at room temperature and the supernatant was removed. Cells were resuspended in 300µL of FACS staining buffer and filtered through a Falcon ® Round-Bottom Tube with a cell strainer cap. Stained cells were detected by BD LSR II flow cytometer at medium speed. Data from the flow cytometer were analyzed by using Kaluza Analysis 2.1.

Gating strategy for panel 1:

1. Cells (SSC-A/FSC-A),
2. Singlets (FSC-H/FSC-A),
3. Live cells (SSC-A/ Viability stain),
4. mTER119 exclusion (SSC-A/mTER119-),
5. Double positive human markers (HLA-ABC/hCD45),

Gating strategy for panel 2:

1. Cells (SSC-A/FSC-A),
2. Singlets (FSC-H/FSC-A),
3. Live cells (SSC-A/ Viability stain),
4. Mouse/human cells (mCD45.1+/hCD45+)

Gated population data were exported, and human engraftment of humanized mice was calculated by the following formula $\frac{human\ cells}{(mouse\ cells+human\ cells)} * 100$.

2.3 Cloning

2.3.1 Gateway Cloning

pDONR221 clones of HDR enhancers and EGFP (synthesized and clone by Thermofisher Scientific or already cloned into pENTR223 prior to master thesis) were aliquoted to 150ng per plasmid. 1 µL of pENTR223 clone, 1 µL of destination vector (pcDNA-pDEST40 (150ng)), and 6 µL of TE (Tris and EDTA) buffer were mixed in a new 1.5 mL Eppendorf tube. LR Clonase™ was thawed on ice and vortexed twice. 2 µL of LR Clonase™ were added to the Eppendorf tube, vortexed, and incubated for 1 hour at 25°C. 1 µL of Proteinase K solution was added, vortexed, and incubated for 10 minutes at 37°C. Mix & Go™ competent *E. coli* cells were thawed, and 20 µL were transferred to new Eppendorf tubes. Between 10 pg to 1000 ng were added to the competent cells, gently mixed, and incubated in ice for 20-30 minutes. After incubation, 250 µL of SOC (Super Optimal broth with Catabolic repression) media was added and plated 50 µL on heated agar plates (Ampicillin or Kanamycin) with a plastic spreader. Kanamycin was used for Ad5, GSE56, Cry1 variants and CYREN and Ampicillin was for i53 and EGFP. The plates were incubated overnight at 37°C with the bottom up. Three colonies were picked from each plate with a loading pipette tip and put in a separate bacterial culture miniprep tube with 5 mL LB media. 100 µg/ml of the Ampicillin or Kanamycin was added, and the cap was put on loosely before being put in an incubator at 37°C 180RPM overnight.

2.3.2 Miniprep

The miniprep procedure was carried out according to the protocol from the ThermoFisher Scientific Miniprep kit.

2.3.3 Maxiprep

The maxiprep procedure was carried out according to the protocol from the ThermoFisher Scientific Maxiprep kit.

2.3.4 Sequencing Miniprep and Maxiprep

Miniprep and Maxiprep samples were prepared accordingly to Eurofins requirements and shipped to Eurofins (https://eurofinsgenomics.eu/) for confirmation of the correct sequence. Sequence analysis was performed by alignment of control and cloned sequences in SnapGene (https://www.snapgene.com/).

2.4 In vitro transcription

In vitro transcription was carried out according to the protocol from HiScribe™ T7 ARCA mRNA Kit (tailing) with some minor modifications. 5000 ng of each HDR enhancer or EGFP was taken into separated Eppendorf tubes and mixed with 2 µL of MssI digestion enzyme, 2 µL of restriction digestion buffer and millQ H_2O in a total reaction volume of 20 µL. The tubes were incubated overnight in 37°C and plasmid linearization was confirmed by electrophoresis of agarose gel for 20 minutes. The working bench and all equipment were sprayed with RNase away and wiped to have it clean and avoiding contamination of RNase. 1000 ng of each linearized plasmid was put in separately clean Eppendorf tubes and mixed with 10 µL of 2xARCA, 2 µL of T7 RNA polymerase mix and millQ H_2O was added to a total volume of 20 µL before incubated for 30 min at 37°C. 2 µL of DNAase enzyme was added to each tube and incubated at 37°C for 15 minutes to remove DNA template. PolyA tail was added to the RNA by adding 10µL of 10x PolyA polymerase reaction buffer, 10 µL of 10X PolyA polymerase and 20 µL of millQ H_2O into each tube making the total volume 50 µL. The mix was vortexed and incubated for 30 min at 37°C. the mRNA was purified by adding 75 µL of LiCl solution to each tube and incubate for 30 minutes at -20°C. After incubation the tubes were the tubes centrifuged at 4°C for 10 minutes. Supernatant was removed and the pellets were rinsed by adding 500 µL of cold 70% ethanol before being centrifuged at 4°C for 10 minutes. The ethanol was removed, and the pellets were air dried for maximum 10 minutes. The pellet was resuspended in 30 µL millQ H_2O until the pellet was not visible. The tubes were

then heated for 10 minutes at 65°C to dissolve the RNA before being measured by Nanodrop. An aliquot of each HDR enhancer mRNA was taken and the rest of the HDR enhancer mRNA was stored in Eppendorf tubes at -80°C. Denaturing gel was made by 1g of agarose and 72 ml of millQ H_2O heated to a clear solution. In a fume hood was 10 mL of 10X MOPS running gel buffer added and 18 mL of 37% formaldehyde (12.3M) added to the agarose before being poured into a chamber and solidified for 2 hours. From the aliquot of in vitro transcribed mRNA was 2000ng pipetted into new clean Eppendorf tubes and mixed with 20 µL of Formaldehyde loading dye and 0.5 µL Ethidium Bromide. The tubes were heat denatured at 70°C for 15 minutes before being loaded into the denaturing gel. The gel was run at 95V for approximately for 1 hour.

2.5 Cell handling

2.5.1 Storage of Healthy Donor Fibroblasts

All the fibroblast cells were deviated from one donor and always stored safely in cryovials at -150°C. One vial contained approx. 2 million cells. This was done for long-term storage.

2.5.1 Cell Counting

For counting, 10 µL of cells and 10 µL of Trypan blue cell counting dye were mixed well in a clean 1.5 mL Eppendorf before being transferred onto Countess cell counting slides.
The cells were counted using automatic cell counter Countess, cell counting slides, and Trypan blue cell counting dye (ThermoFisher Scientific)

2.5.2 Thawing Human Fibroblasts

Every procedure was done in a sterile BL-2 laminar hood. Before anything entered the hood, it was sprayed with 75% ethanol and wiped off with paper towels. Cells were transported in Styrofoam boxes filled with dry ice. The cells were thawed by holding the vails in a water bath at 37°C for 1 minute. Before the entire vail was thawed, was it transported into the hood, and before 1 ml RT thawing medium (without antibiotics) was gently added to the vial. The vial was poured into a 15mL falcon tube with thawing media warmed to 37°C. Then, the cells were centrifuged at 1400 rpm for 5 minutes, and the pellet was gently resuspended and transferred to a pre-heated

culture flask containing a 30 ml primary fibroblast culture medium. The flask was stored at 37°C in an incubator with 5% CO_2

2.5.3 Splitting cells

When the cells had reached 90% confluency, the cell culture media was removed, and the cells were washed with pre-warmed 1x PBS to remove medium or dead cells. Pre-heated Trypsin was added to detach the cells and incubated for 5 minutes at 37°C before being inspected under the microscope. Pre-warmed cell culture media was added to dilute the trypsin; the cell suspension was transferred to a 50 mL falcon tube and centrifuged at 1400 rpm for 5 minutes. The supernatant was discarded before 20 mL of cell culture media was added and resuspended the pellet. To count the cells, an aliquot of 10 µL cells was taken and mixed with 10 µL of trypan blue. The cells were then split into four new flasks with cell-cultured media and again placed in an incubator.

2.6 HDR Enhancer Experiment in Fibroblasts

2.6.1 Cell Preparation for Electroporation

The cell culture media was removed, and the cells were washed with pre-warmed 1x PBS to remove medium or dead cells. Pre-heated Trypsin was added to detach the cells and incubated for 5 minutes at 37°C before being inspected under the microscope. Pre-warmed cell culture media was added to dilute the trypsin; the cell suspension was transferred to a 50 mL falcon tube and centrifuged at 1400 rpm for 5 minutes. The supernatant was discarded, and 20 mL of 1x PBS was added before the pellet was resuspended. A 10 µL aliquot was taken for counting cells, and the numbers from cell counting were calculated, so it was approximately 1 million cells to each vail. The cells were centrifuged, and the supernatant was discarded.

2.6.2 Preparation of Ribonucleoproteins (RNP) complexes

In a sterile BL-2, 100 pmol of ADA2 sgRNA nr. 3 was pipetted into 96 well PCR plate. Cas 9nuclease, batch YY produced by Karolinska Institute, was thawed on ice, and 61pmol was pipetted into the same wells containing ADA2 sgRNA nr. 3. Both Cas9 and sgRNA were mixed gently, the plate was sealed and spun down by a plate spinner. The plate was incubated for 15

minutes at room temperature before adding 100 pmol of ADA2 forward ssODN repair template onto the RNP complex. The plate was sealed, spun, and then stored on ice until the electroporation procedure

2.6.3 Electroporation

Prepared cells (500 000 – 1 000 000) were resuspended in 20 µL of Lonza electroporation buffer (20 µL per electroporation well) and transferred onto the RNP complexes. mRNA was pipetted accordingly to concertation in each selected well, plate was sealed, and spun down. 20 µL of the cell-RNP-mRNA mix were loaded onto an electroporation strip before being inserted into Lonza 4D- nucleofector system (software 2.1). Mock electroporation sample was included without any RNPs and only RNP condition without any mRNA was implemented. As for mRNA control, EGFP mRNA was used.

Electroporation program:

- Primary Cell P3
- Pulse code CA-137

After the electroporation, the electroporation strip was removed, and 80 µL of pre-warmed recovery medium was added before incubation for 15 minutes at 37°C. The cells were then transferred from the electroporation strip into prepared cell-cultured 6- well plates with recovery media. The cells suspension was gently rocked to be evenly distributed.

Twenty-four hours later, the recovery media was aspirated and replaced with fibroblast culture media supplemented with antibiotic P/S. The cells were collected 4 days post electroporation. The cell culture media was removed, and the cells were washed with pre-warmed 1x PBS to remove medium or dead cells. Pre-heated trypsin was added to detach the cells and incubated for 5 minutes at 37°C before being inspected under the microscope. Pre-warmed cell culture media was added to dilute the trypsin. The cell suspension was transferred to a clean 1.5 ml Eppendorf tube and centrifuged at 1400rmp for 5 minutes. The supernatant was removed and washed once with 1x PBS. The cells were centrifuged, 1x PBS was removed, and the cell pellet was stored at -20°C until DNA isolation

RNP mix sequence:

ADA2 sgRNA #3 (Red letters indicate PAM)

5` - TGCTGGAGGATTATCGGAAG CGG - 3`

ADA2 repair template (ssODN) forward (Red letters are introduced silent mutation)

5`-
CCCCGTCCATCAGAAAAATGTTCCAAGTGGATTCTGCTGGAGGACTACAGAAAG
CGGGTGCAGAACGTCACTGAGTTTGATGACAGGTGAGTAGTAGTTC -3`

2.6.4 DNA isolation

DNA purification was carried out by following Qiagen protocols for QIAmp® 96 QIAcube® HT Kit.

2.6.5 ddPCR

DNA concentration measured from DNA purification was normalized to 4 ng/µL in 20µL. A master mix for NHEJ and HDR with a primer probe was made (Table 2). In 96 well plate, 8 µL of the normalized DNA sample was pipetted into two separate wells. Onto the wells, 12 µL of HDR master mix was added to one and 12 µL of NHEJ master mix was added to the other. The 96 well plate was loaded into an automated droplet generator. After the droplets generator was completed, the plate was heat-sealed at 170°C and transported to a PCR machine with the following program

1. 95°C – 10 minutes
2. 94°C – 30 seconds
3. 56°C – 3 minutes
4. 98°C – 10 minutes
5. 4°C – Hold

Repeated 42 times

After PCR was completed the 96 well plate was transported to the Droplet reader and lunched QuantaSoft on the computer. In the software the plate-reading parameters were selected.

Experiment: RED
SupperMix: ddPCR Supermix for Probes (no dUTP)
Target1, Type: Ch1 Unknown
Target1, Type: Ch2 Unknown

Data from the droplet reader were then gated in a 2D Amplitude plot in QuantaSoft.

Sequences for ADA2 ddPCR master mixes:

- primer forward 5`-GGT GAG GAA TGT CAC CTA CA -3`
- primer reverse 5`-GTA CCA AGG GAG ACA CCT AC -3`
- FAM 5`-/56-FAM/GCC ACA TCT GTT TCA CCC CA/3BHQ_1/-3`
- NHEJ probe 5`-/5HEX/ATT ATC GGA AGC GGG TGC AGA /3BHQ_1/-3`
- HDR probe 5`-/5HEX/CTG GAG GAC TAC AGA AAG CGG /3BHQ_1/-3`

Table 2: Master mix volumes for NHEJ and HDR. *Tables are setup for one sample (n = 1). Mixes were prepared in two separate Eppendorf tubes according to calculations.*

Master mix (NHEJ)	n = 1
ddPCR mix	10
FAM-NHEJ + HEX with primers	1
H2O	1
FAM-NHEJ + Hex with primers:	n = 1
primer fwd ADA2	0.18
primer rev ADA2	0.18
FAM (NHEJ probe)	0.05
HEX (reference probe)	0.05
H2O	0.54
sum	1

Pipetting (HDR) ADA2	n = 1
ddPCR mix	10
FAM-HDR + HEX with primers	1
H2O	1
FAM-HDR + Hex with primers:	n = 1
primer fwd ADA2	0.18
primer rev ADA2	0.18
FAM (HDR probe)	0.05
HEX (reference probe)	0.05
H2O	0.54
sum	1

2.8 Statistical Analysis

Statistical analysis was done using Microsoft Excel or GraphPad Prism 9 (GraphPad Software Inc). Values are shown by mean +- standard deviation. For statistical testing, a parametrical two-tailed t-test was used. Asterisks shows ≥ 0.05 not significant (ns), 0.01 to 0.05 significant (*), 0.001 to 0.01 very significant (**).

3 Results

3.1 Human Engraftment in SCID Mice

3.1.1 Weight Monitoring

45 mice separated into five treatment groups were irradiated before intravenous injection containing with edited or unedited hematopoietic stem progenitor cells (HSPCs) (Table 1). Bodyweight changes were monitored by weighing the mice weekly. A general trend was a reduction of weight the week following irradiation. These mice were observed to have a loss of appetite (Figure 9). Treatment groups 3A and 1A were injected with unedited HSCs and were supposed to be used as a control for mice injected with edited HSPCs. However, many mice in this group died before the experimental end date, which was set to week 16 post-irradiation but got changed to week 12. We experienced many deaths between week 2 and week 11 in both edited and unedited groups. During this time frame, 16 mice in the unedited groups (1A, 3A; Figure 9A, D) and 12 mice in the edited groups (2A, 2B, 3B; Figure 9B, C, and E) were lost. While some of these mice were euthanized due to post-irradiation sickness symptoms, e.g., pain, lethargy, cold, apathy, rapid weight loss, and diarrhea, most of the deaths occurred unexpectedly, as healthy-looking mice would be found dead the next day. In addition to deaths in the treatment groups, one out of three mice in the control group, which contained non-irradiated mice injected with PBS instead of HSPCs, were found dead in week 5 (Figure 9F). The weight in week 12 is not representative of the actual weight but just to show which mice survived to the end.

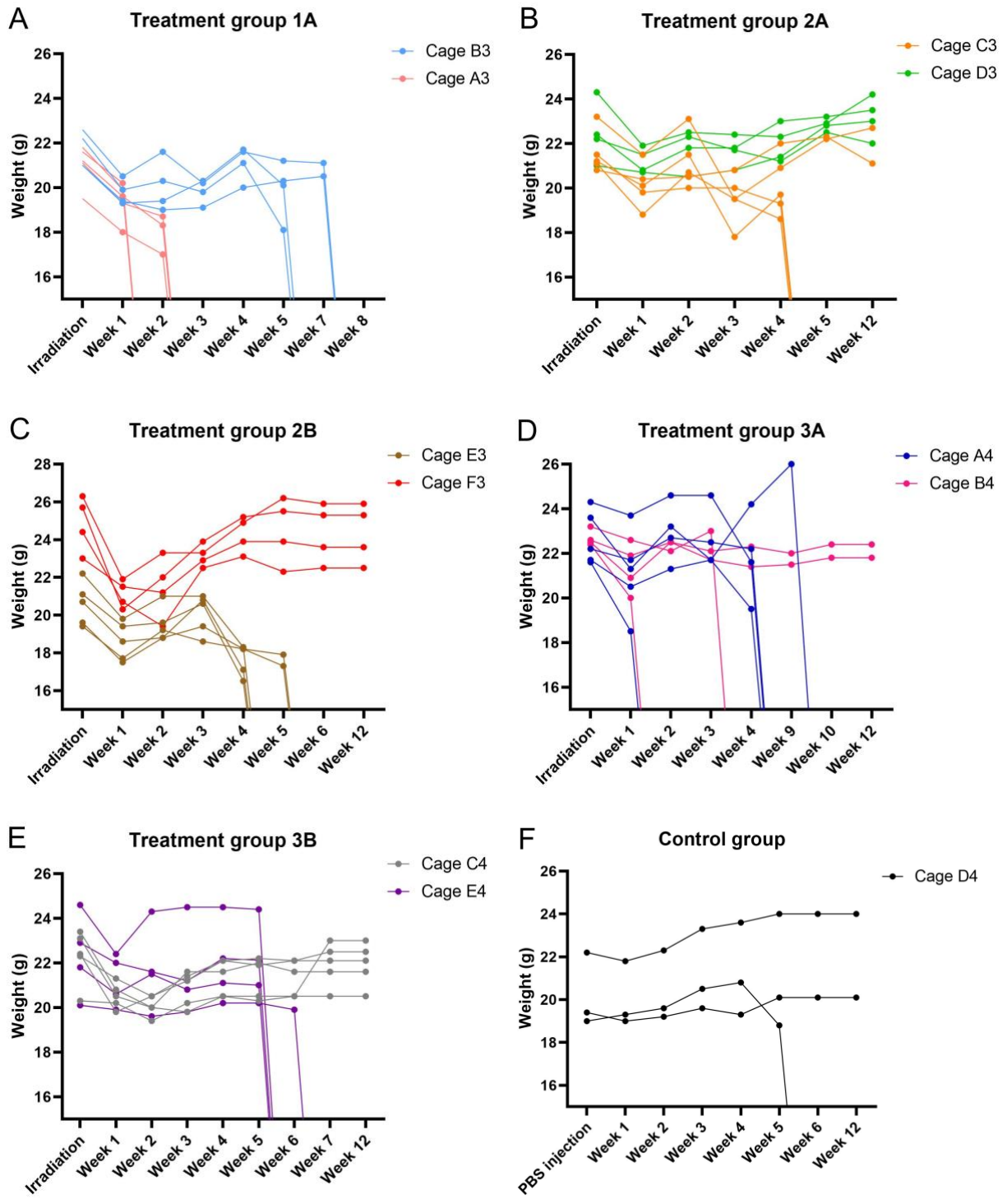

(See figure on the previous page)

Figure 9. Overview of the weight progression of mice post-irradiation. *Graphs show weight of mice in treatment groups (1A, 2A, 2B, 3A, 3B) and control group over the course of the experiment (12 weeks). Y-axis shows the weight*

from 15g up to 28g due to the individual mouse to mouse variation. The X-axis show weight measured each week, starting from the day of irradiation until the end of the experiment or day when the mouse was found dead/sacrificed. Mouse death (unexpected or euthanized) is indicated by a complete drop in weight (0g). Each treatment group contained nine mice divided into two cages (4 and 5 mice per cage). ***A)*** *Treatment group 1A (unedited HSCs from AllCells). The first mouse was found dead in week 1. All mice were found dead by week 8.* ***B)*** *Treatment group 2A (edited HSCs from AllCells). Three mice were found dead in week 4.* ***C)*** *Treatment group 2B (edited HSPCs from AllCells). All mice in cage E3 died between week 4 and 6.* ***D)*** *Treatment group 3A (unedited HSCs from local donor). The first mouse was found dead by week 2. All mice in cage A4 were found dead by week 10.* ***E)*** *Treatment group 3B (edited local donor HSCs). The first mouse was found dead in week 5. All mice in cage E4 cage died between week 5 and 7.* ***F)*** *Control group (injected with PBS only without irradiation step). One mouse was found dead in week 5.*

3.1.2 Cell Count and Viability Assay

All mice lost before week 11 were referred to as unfinished-experiment mice (UE mice), while mice finishing the experiment in the designed human endpoint (12 weeks) were referred to as finished-experiment mice (FE mice). Bone marrow was harvested from the UE mice. Cells were extracted from the bone marrow and analyzed by flow cytometry. From the flow cytometer data would we look for the human engraftment which is the reproducing transplanted human HSC. UE mice lost in week 5 had low human engraftment, ranging from 2 to 10%. >10%. Therefore, less than 10% of human engraftment in the bone marrow was defined as failed bone marrow engraftment. Data from UE mice were therefore not included in the results.

FE mice were euthanized at week 12. Bone marrow, spleen, and peripheral blood from these mice were collected. Cells harvested from the bone marrow and spleen were counted, and their viability was measured (Figure X). We did not measure the viability or count the cells of the peripheral blood because the amount of collected volume was low, ranging from 100 to 500 mL of blood per mouse, and we wanted to preserve as many cells for flow cytometry analysis. Data from four mice in treatment group 2A bone marrow was unfortunately lost due to logistical and data handling.

The different treatment groups had a lot of variation in both bone marrow and spleen cell count. The total number of cells in the bone marrow ranged from $5x10^5$ to $6.2x10^7$ (Figure 10A). Treatment group 2B, which contained edited bought HSCs (AllCells), had the highest bone marrow cell count. Group 3B, which contained edited HSC (local donor), in addition to the control group, had the lowest bone marrow cell count. Treatment group 3B and the control group had the

lowest number of spleen cells as well (Figure 10B). The number of spleen cells in 3B ranged between $1.7x10^6$ to $5.3x10^6$ cells, while in the control group, there were as few as $6.3\text{-}8.7x10^5$ cells. We observed high amount of spleen cells in several groups. Treatment group 2B had up to $8.8x10^7$ cells and a mean of $6.2x10^7$ cells, and treatment group 3A had a mean of $7.1x10^7$ cells. In general, there were more cells harvested from the spleen than bone marrow.

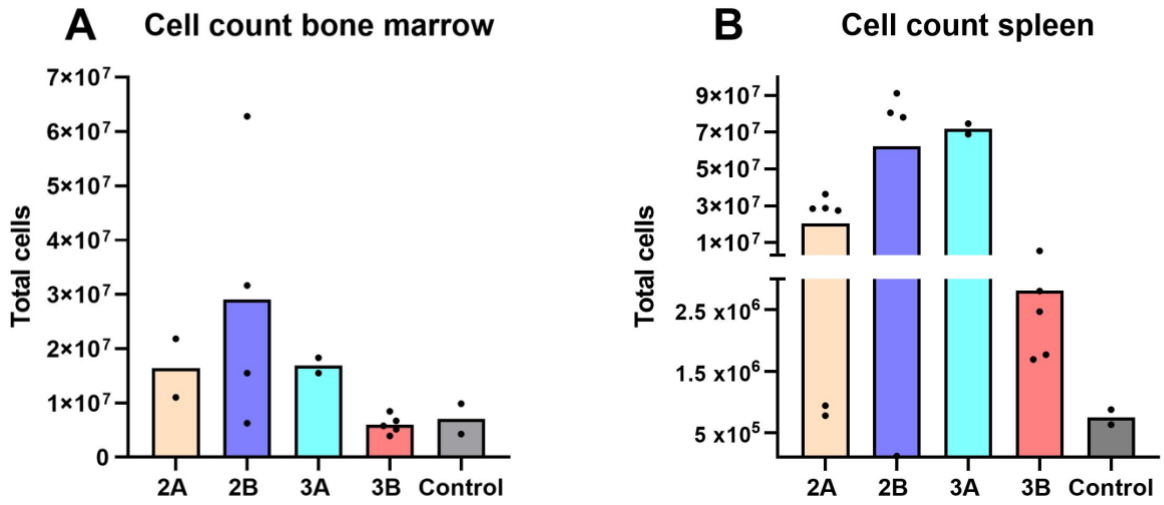

Figure 10. Overview of number of cells collected from mouse bone marrow and spleen.

Graphs of A) The total number of extracted cells from bone marrow, B) the total number of extracted cells from the spleen. Graphs include data from mice in treatment groups 2A, 2B, 3A, 3B, and control. Data from 4 mice in treatment group 2A was lost in A).

3.1.3 Human Engraftment in Bone Marrow, the Spleen and Peripheral Blood

The cells harvested from the bone marrow and spleen had overall high viability, ranging from 59% to 99% (Figure 11). Bone marrow cells had the highest viability. All individuals in the groups had viability above 80% in cells of the bone marrow (Figure 11A). The lowest viability was found in cells of the spleen of the control group, where the mean viability was 65.5%. Apart from treatment group 3B, which had a mean of 78% viability, all treatment groups had viability mean above 80% in the spleen cells (Figure 11B).

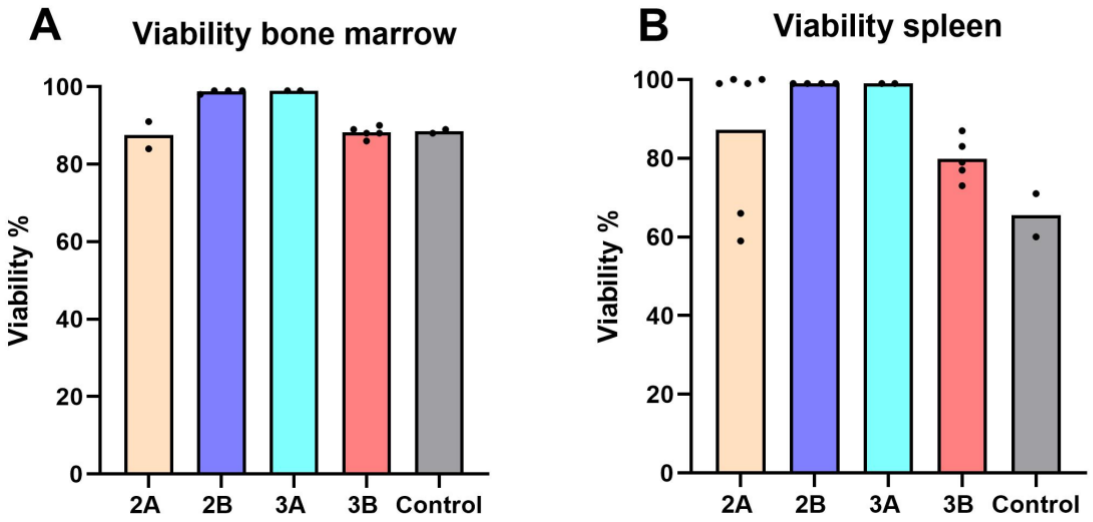

***Figure 11*. Overview of the viability of cells collected from mouse bone marrow and spleen.**

Graphs of A) the percentage of viable cells extracted from bone marrow and B) the percentage of viable cells extracted from the spleen. Graphs include data from mice in treatment groups 2A, 2B, 3A, 3B, and control. Data from 4 mice in treatment group 2A was lost in A).

After cell counting and viability analysis, human engraftment was confirmed by identifying $hCD45^+$ cells in the spleen, peripheral blood, and bone marrow using flow cytometry analysis. Cells from all three organs were stained with panel 1 antibodies. Bone marrow cells were additionally stained with panel 2 antibodies. To confirm human engraftment in cells stained with panel 1 antibodies, the following gating strategy was applied (Figure 12-14): cells outside the gate in a side scatter area (SSC-A) against a forward scatter area (FSC-A) plot were assumed to be cell debris. Within the cells gate, singlets were gated in a forward scatter height (FSC-H) against FSC-A plot to exclude non-singlets. Doublets and clusters had a larger area-to-height ratio than singlets and were left out of the gate. Next, viability was checked by plotting the viability marker Aqua Live/Dead in a Pacific orange-A channel against SSC-A. The live cells were in the left gate, without releasing fluorescence signal compared to the dead cells. Within the live cell gate, mouse erythrocytes were excluded by plotting SSC-A against the mouse cell marker mTER119 (PE-Cy5-A). mTER119 negative cells were gated for further analysis (Figure XD). Within the mTER119 negative gate, SSC-A was plotted against the mouse cell marker mCD45.1 (PE-Cy7-A) to identify gated $mCD45.1^+$ mouse cells. Lastly, within the mTER119 negative gate, HLA-ABC (Alexa Flour 700-A) was plotted against hCD45 (Pacific Blue-A) (Figure XF). Both being human markers,

HLA-ABC$^+$ hCD45$^+$ cells were identified as human cells and indicated successful human engraftment. All gates were set up using unstained controls and compensation for all used antibodies was performed previously.

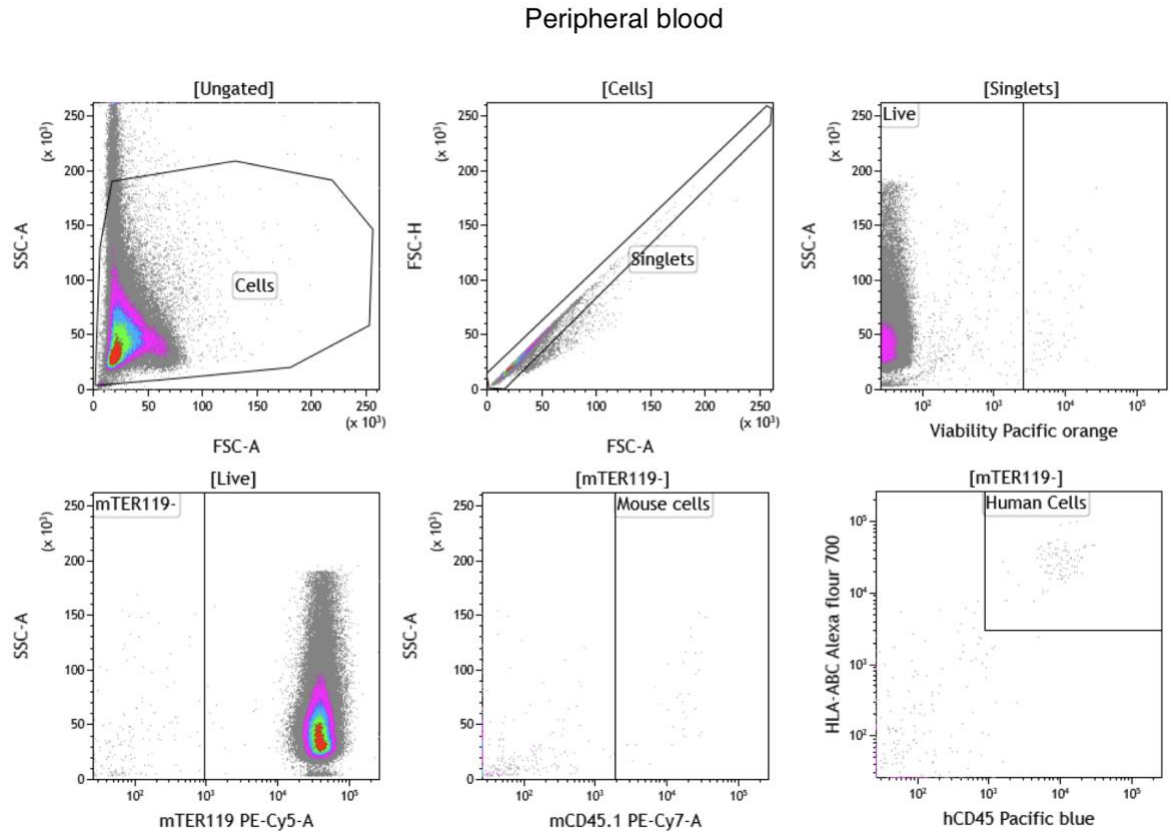

Figure 12. Gating strategy to confirm engraftment of human hematopoietic stem cells in mice-derived peripheral blood cells stained with panel 1. *Flow cytometry dot plots showing gating of: cells identified by SSC-A vs FSC-A (upper left panel), singlets identified by FSC-H vs FSC-A (upper middle panel), live cells identified by SSC-A vs Viability (upper right panel), mTER119- cells identified by SSC-A vs mTER119 (lower left panel), Mouse cells identified by SSC-A vs mCD45 (lower middle panel), Human cells identified by double positivity in HLA-ABC vs hCD45 (lower right panel) to confirm human engraftment in mouse peripheral blood. (Mouse id F3-2).*

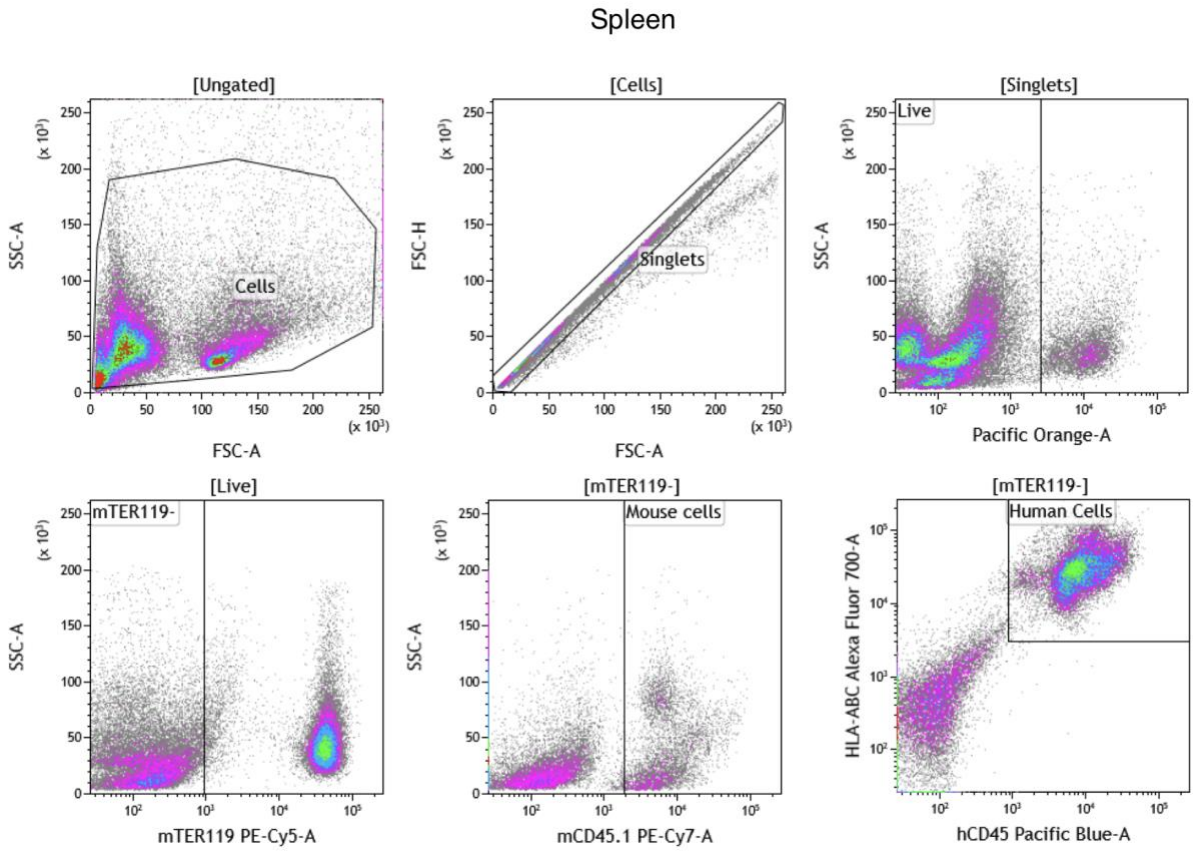

Figure 13. Gating strategy to confirm engraftment of human hematopoietic stem cells in mice-derived spleen cells stained with panel 1. *Flow cytometry dot plots showing gating of: cells identified by SSC-A vs FSC-A (upper left panel), singlets identified by FSC-H vs FSC-A (upper middle panel), live cells identified by SSC-A vs Viability (upper right panel), mTER119- cells identified by SSC-A vs mTER119 (lower left panel), Mouse cells identified by SSC-A vs mCD45 (lower middle panel). Human cells identified by double positivity in HLA-ABC vs hCD45 (lower right panel) to confirm human engraftment in mouse spleen. (Mouse id F3-2).*

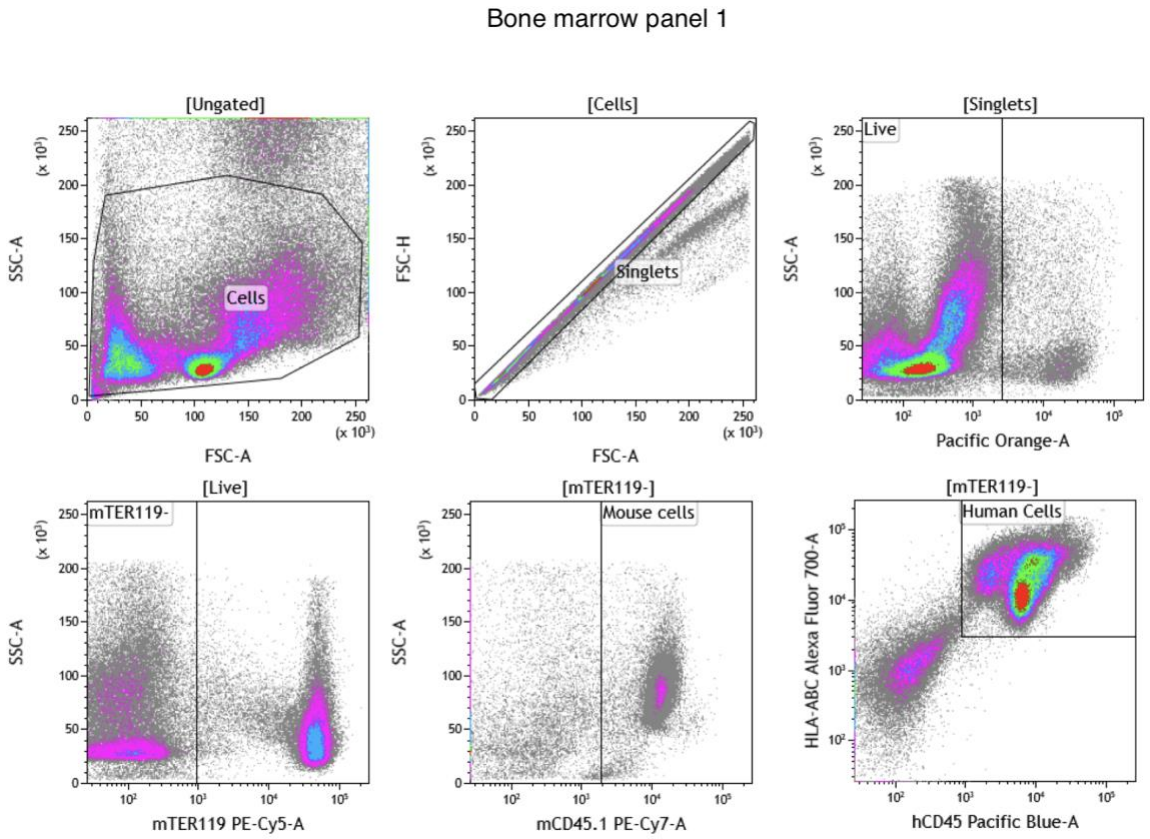

Figure 14. Gating strategy to confirm engraftment of human hematopoietic stem cells in mice-derived bone marrow cells stained with panel 1. *Flow cytometry dot plots showing gating of: cells identified by SSC-A vs FSC-A (upper left panel), singlets identified by FSC-H vs FSC-A (upper middle panel), live cells identified by SSC-A vs Viability (upper right panel), mTER119- cells identified by SSC-A vs mTER119 (lower left panel), Mouse cells identified by SSC-A vs mCD45 (lower middle panel), Human cells identified by double positivity in HLA-ABC vs hCD45 (lower right panel) to confirm human engraftment in mouse bone marrow. (Mouse id F3-2).*

Human engraftment in bone marrow cells stained with antibodies from panel 2 was confirmed by applying a gating strategy without second human marker, HLA-A, B, C, and mouse marker mTER119 (figure 15). The second gating strategy was used to test whether a simpler gating strategy would give similar engraftment results. Panel 2 stained cells were gated for in an SSC-A against FSC-A plot. Within the cells gate, singlets were gated in an FSC-H against FSC-A plot. Live cells were then gated in an Aqua Live/dead in a Pacific orange-A channel against an SSC-A plot. Next, human and mice cells were gated for in mCD45.1 (PE-A) against hCD45 (BV711-A) plot. Successful human engraftment in the bone marrow was indicated by $mCD45.1^{-}hCD45^{+}$ cells.

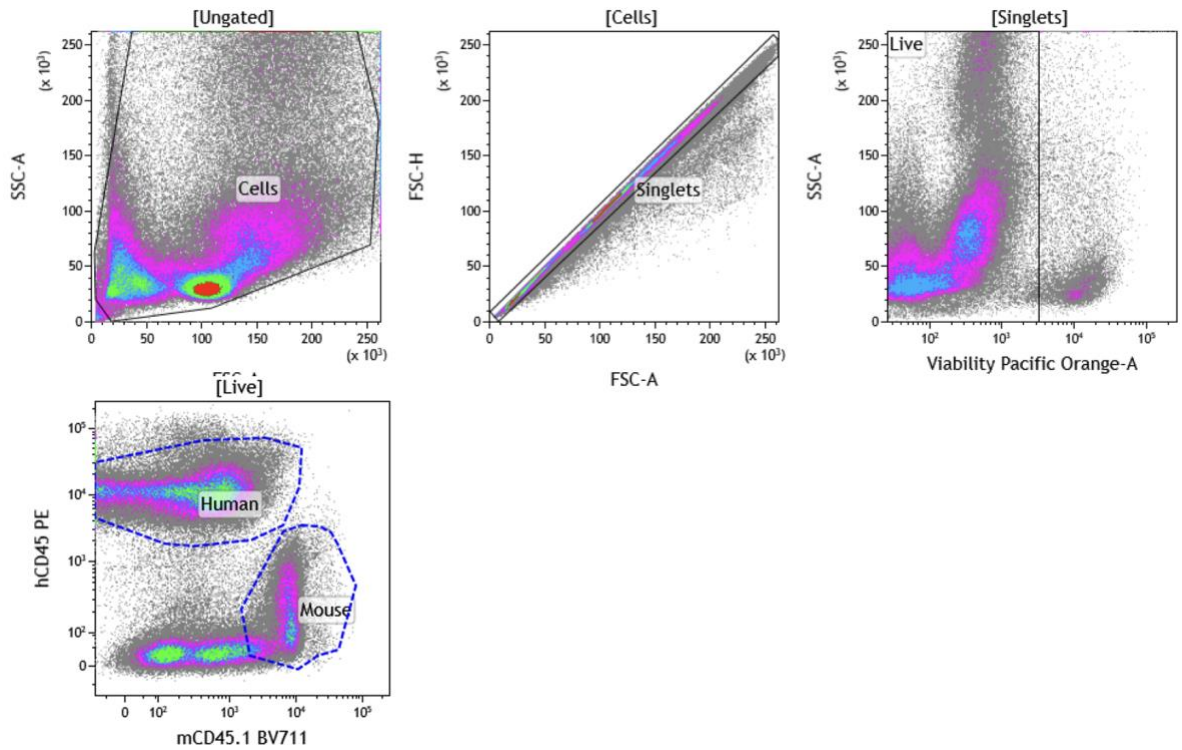

Figure 15. Gating strategy to confirm engraftment of human hematopoietic stem cells in mice-derived bone marrow cells stained with panel 2. *Flow cytometry dot plots showing gating of: cells identified by SSC-A vs FSC-A (upper left panel), singlets identified by FSC-H vs FSC-A (upper middle panel), live cells identified by SSC-A vs Viability (upper right panel), human and mouse cells identified by mCD45.1 vs CD45 (lower panel) to confirm Human engraftment in mouse bone marrow. (Mouse id F3-2).*

Engraftment results of the peripheral blood were highly varying, ranging between 5 to 74% among the different treatment groups (Figure 16A). Most individuals had between 10-30% human engraftment in peripheral blood. Human engraftment in the spleen varied between the different treatment groups (Figure 16B). While treatment group 3B had the lowest mean percentage of engraftment (22%), treatment group 2B had the highest mean of engraftment (56%). We observed variance in spleen engraftment among the individuals in 2A. Two of the mice in this group had 58% and 64% engraftment, another had 4%, and the three remaining individuals ranged between 15% and 33% respectively.

The results for HSC engraftment in the bone marrow did not vary much when comparing the two tested gating panels. The panel 2 gating strategy proved to be somewhat less specific and more specific than panel 1, as the percentages of engraftment overall were slightly higher when gating

using panel 2 (Figure 16C). Treatment group 2A had the lowest mean percentage of human engraftment in the bone marrow. Although two of the individuals in the group had 57% and 68% engraftment, the four of the mice had 10-33%. Treatment groups 2B and 3B were the groups with the highest mean percentage of human engraftment, 67 and 70% respectively. Overall, we observed the highest human engraftment in the bone marrow compared to the spleen and peripheral blood compartments.

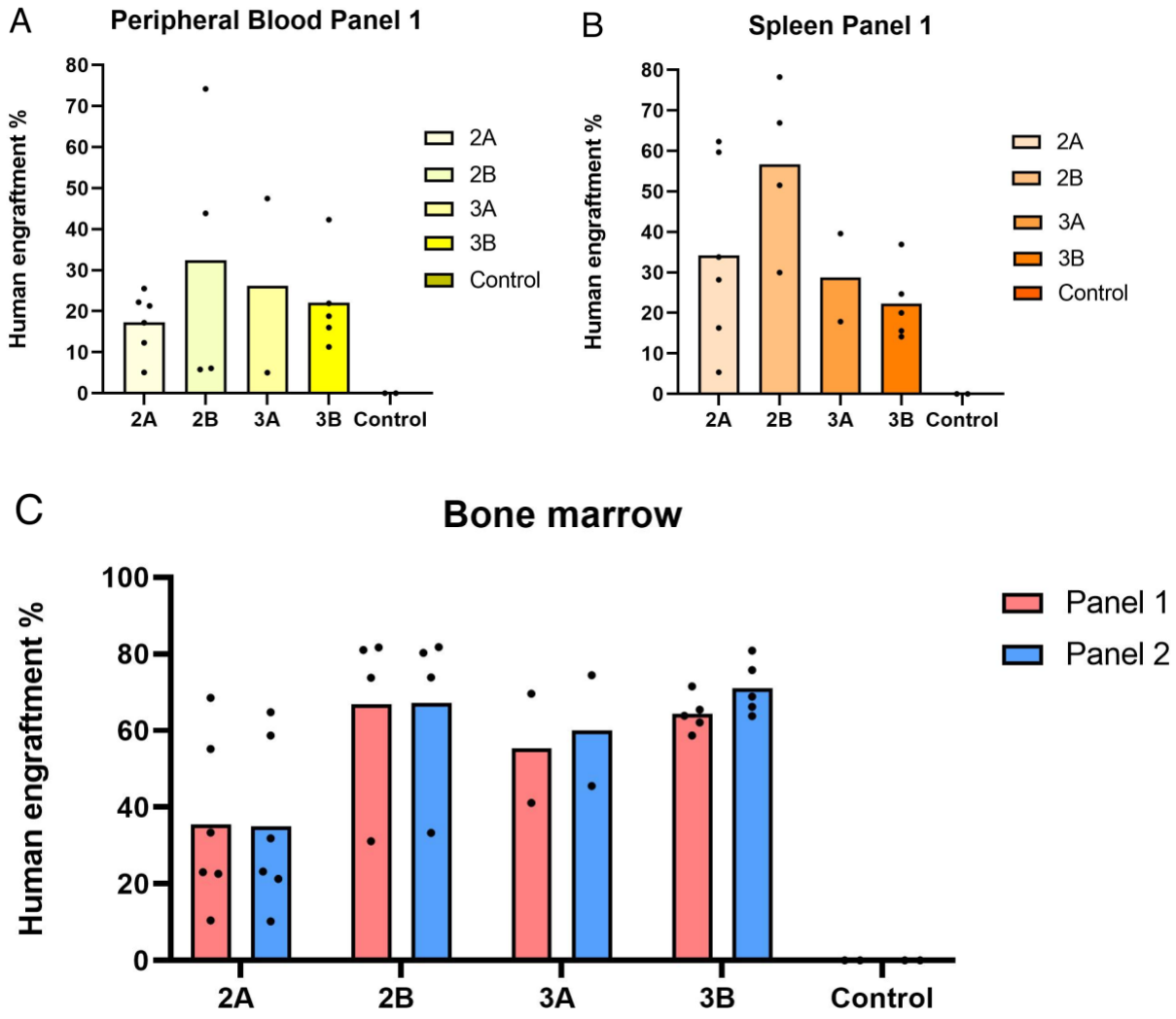

Figure 16. Percentage of human stem hematopoietic cells engraftment in peripheral blood, spleen, and bone marrow. *A) Comparison of human engraftment between the treatment groups (2A, 2B, 3A, 3B, and control) in peripheral blood. B) Comparison of human engraftment between the treatment groups in the spleen. C) Comparison of human engraftment between the treatment groups in bone marrow confirmed by panel 1 and panel 2 gating. All comparisons in graphs in A-C were non-significant.*

3.2 Testing of HDR Enhancers

To optimize precise gene editing, we aimed to reduce the events of NHEJ and increase the events of HDR. NHEJ is the canonical DSB repair pathway. NHEJ is quick, template free, and not limited to a cell cycle phase. On the other hand, HDR is time demanding, functions to incorporate a donor template, and is limited to the S/G_2 phase of the cell cycle [56]. To block the NHEJ pathway and force the cell to repair the double-strand break by HDR, we added various HDR enhancers to a ribonucleoproteins (RNP) complex (Cas9 YY protein, ADA2 sgRNA WT #3, and HDR forward repair template). We tested 5 HDR enhancers: Genetic suppressor element (GSE56), Adenovirus 5-E4orf6/7 (Ad5), cell cycle regulator of non-homologous end joining (CYREN), three versions of Cry 1, and an inhibitor of 53BP1 (i53). The latter (i53) functions to temporarily inhibit the accumulation of 53BP1, a transcription factor essential for NHEJ, at the induced double-strand break site [56]. Additionally, we used i53 combined with FLAG to test if it would improve mRNA stability. E2F transcription factors to enable entry into the S-phase of the cell cycle. GSE56 was shown as a direct inhibitor p53, thus increasing the frequency of HDR [61]. CYREN is a cell-cycle-specific inhibitor of NHEJ, as it binds Ku70/80 to restrict NHEJ proteins from binding their docking sites at the double-strand break [36, 62]. The cryptochrome 1 (Cry1) is a factor in circadian rhythm. Cry1 has a regulator role in DNA repair processes and in cell proliferation. Homologous recombination (HR) factors are promoted by the binding of Cry1 which are regulating HR DDR [63]. Three different variants of Cry1 were tested in this experiment, Cry1 without (WO) NLS, Cry1 5´end NLS, and Cry1 3´end NLS.

3.2.1 Cloning HDR enhancer

Each of the entry clones (HDR enhancers) was cloned into the destination vector pDEST40. Bacterial transformation of the products was necessary to maintain an appropriate plasmid stock. Cultured colonies we performed Miniprep on before the product was sent to sequencing to verify the correct sequence. A new round of bacterial transformation with the confirmed miniprep colonies was cultured in a larger volume to perform Maxiprep. Verification of the Maxiprep colonies was carried out and the confirmed product was ready for the next step.

3.2.2 mRNA production

Before testing the HDR enhancers described above, their mRNA was prepared by performing IVT from plasmids suitable for IVT since plasmids are toxic to primary cells [64]. Ad5, i53, and GSE56 mRNA were tested alone in a titration experiment with concentrations of 500ng, 1000ng, 2000ng, and 3000ng. Titration was done to evaluate if increased concentration would be toxic for the cells and find the optimal concentration for each of them. In addition to HDR enhancers, IVT was also performed to enhanced green fluorescent proteins (EGFP), which were used as a control for mRNA for the following experiments. The electrophoresis experiments were successful, as clear mRNA bands were seen in most lanes (Figure 17). In lanes where several bands were observed, the brightest bands corresponded to HDR enhancer mRNA, while less bright bands (much shorter) were artifacts resulting from the IVT reaction, having no effect on the experiment. (Figure 17C-D). IVT was performed twice for EGFP and i53 since we were unsure if the first experiment was done correctly. A smeared band observed in one of the EGFP lanes confirmed this, as the smearing indicated degraded mRNA product (Figure 17C, far-right band). Clear bands seen from the gel electrophoresis confirmed intact and compact mRNA of all HDR enhancers. Also, we observed high yield of mRNA production after measuring the RNA concentration using Nanodrop.

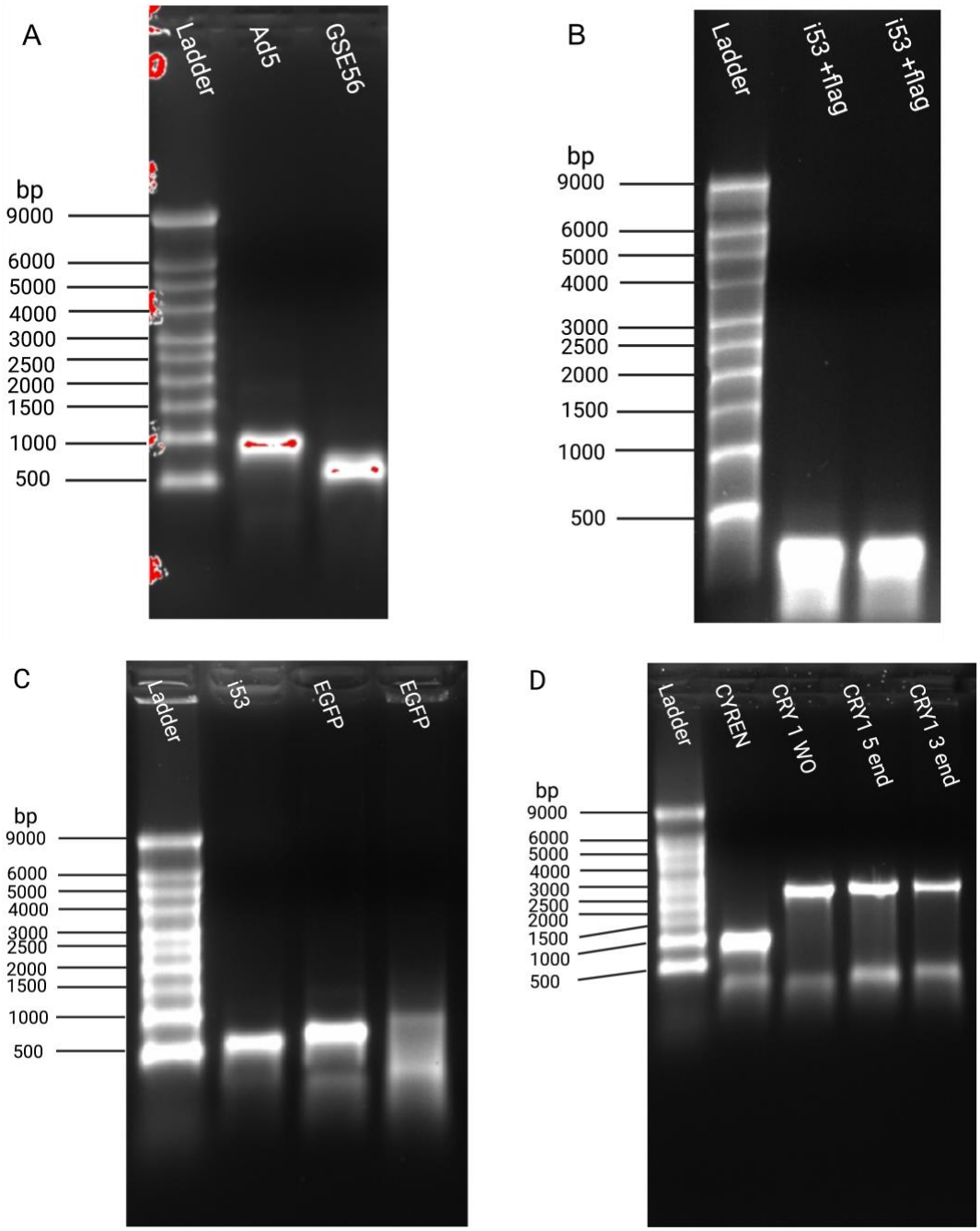

Figure 17. mRNA quality assessment of IVT reaction by denaturing formaldehyde gel electrophoresis.

Electrophoresis gel images after IVT reaction. An mRNA ladder was used to confirm the mRNA product of HDR enhancers by sequence size (bp). Smaller products migrated further through the gel than larger products, which is indicated by the values of the bands of the ladder. The brightest band correlates to mRNA. Less bright bands in the same lane are artifacts. A) (from left) ladder, GSE56 (1000bp), and Ad5 (600bp). B) (from left) ladder, i53Flag(400bp), and i53Flag (400bp). C) (from left) ladder, i53 (550bp), EGFP-1 (800bp), and EGFP-2 (NA). D) (from left) ladder, CYERN (1000bp), Cry1 WO (3000bp), Cry1 5´end NLS (3000bp), and Cry1 3´end NLS (3000bp).

3.2.3 Testing Single HDR Enhancers in Fibroblasts

After electrophoresis, mRNA concertation of the various HDR enhancers and controls were measured and the amount of RNA needed for transfection by electroporation was calculated (Table 2).

***Table 2. Results from IVT with mRNA concentration measured with Nanodrop**. The amount of needed mRNA was calculated for further testing. Each concentration is shown in ng where the volume below is shown in µL*

Sample	Concentration ng/µL	500 ng (µL)	1000 ng (µL)	2000 ng (µL)	3000 ng (µL)
Ad5	1198	0,42	0,83	1,67	2,50
i53	1252	0,40	0,80	1,60	2,40
i53 + flag	1000	0,50	1,00	2,00	3,00
GSE56	1077	0,46	0,93	1,86	2,79
Cyren	913	0,55	1,10	2,19	3,29
Cry1 WO	1049	-	-	-	2,86
Cry1 NLS 5´end	812	-	-	-	3,69
Cry1 NLS 3´end	1136	-	-	-	2,64
EGFP	1400	-	0,71	-	-

The fibroblast cells which were prepared before electroporation was all from the same donor (C27-1) and from the same passage (number 4). Delivery of the RNP complexes, which refers to RNP mix + mRNA of HDR enhancer, to fibroblasts was performed successfully by electroporation. Four days later, the cells were collected, DNA isolated and subjected to ddPCR to analyze editing outcomes. HEX fluorochrome is a general DNA binder for both NHEJ and HDR events. FAM-NHEJ is a specific DNA binding fluorochrome for a specific sequence in ADA2 locus. An indel in this specific sequence would influence the binding affinity of the specific DNA binding fluorochrome.

For electroporation experiments measuring NHEJ events, binding of both FAM and HEX (FAM+/HEX+) labeled probes indicated both probes were able to bind the DNA and there were no indels introduced to the sequence, and therefore no change in DNA sequence. Thus, NHEJ did not occur. Binding of HEX probe only (FAM-/HEX+) on the other hand suggested NHEJ had occurred, as FAM probe would not be able to bind the target site in the presence of an indel. Most of the droplets were HEX+ and located along the area of 4000 to 5000 channel 1 amplitude on the

y-axis (Figure 18). Droplets also located between 1000 to 3000 channel 2 amplitude on the x-axis were FAM-. Moving further right along the x-axis, the droplets were positive for FAM with low affinity, indicating minor DNA alterations. All droplets with lower affinity than that of the wild type were suggested to have undergone NHEJ and can be seen as blue dots.

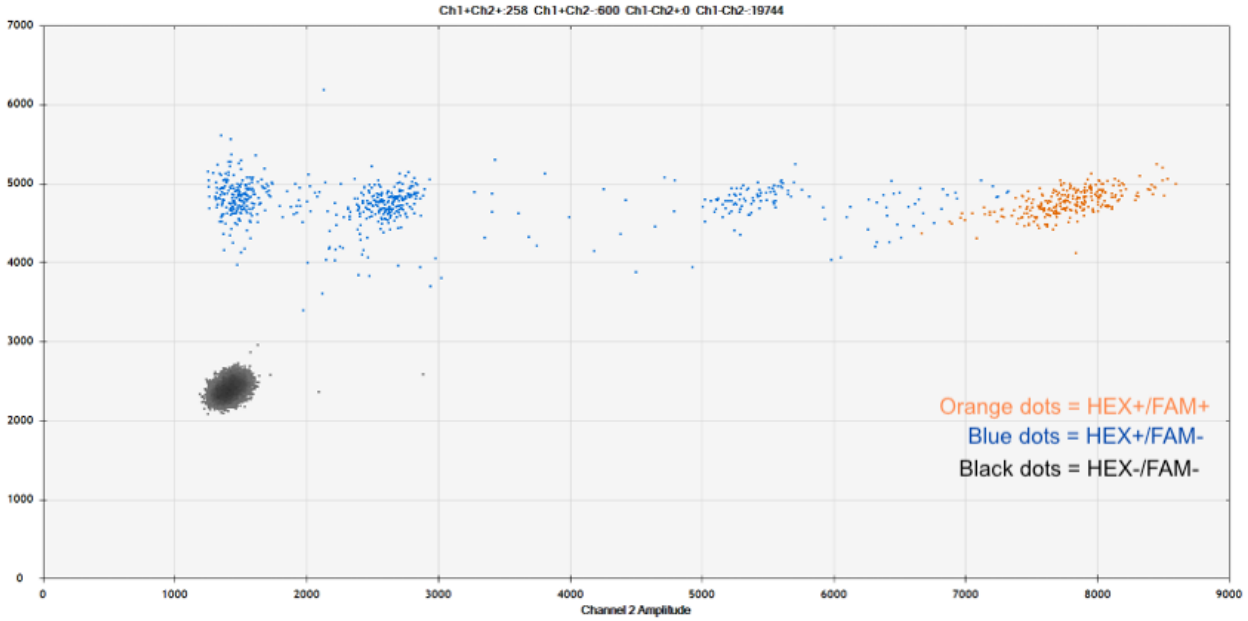

Figure 18. NHEJ gating in electroporated fibroblast with i53 HDR enhancer

The plot shows a two-dimensional cluster in which channel 1amplitude fluorescence (FAM-NHEJ probe) is plotted against channel 2 amplitude (HEX probe). In the HEX+/FAM- population) the reference DNA-binding HEX- probe had bound while the unedited DNA-binding FAM-NHEJ probe had not, indicating NHEJ indels. Decrease in FAM-NHEJ affinity to DNA would place the dots in a lower amplitude in channel 2. The HEX+/FAM+ population (orange dots) had bound both the reference DNA-HEX probe and the unedited DNA-FAM probe, indicating NHEJ indels had not occurred. The HEX-/FAM- population (grey dots) indicated no probes had attached to the DNA.

For electroporation experiments measuring HDR events, binding of both FAM-HDR and HEX (FAM+/HEX+) indicated HDR events had occurred. While HEX binds DNA of the ADA2 locus in general, FAM-HDR is a specific probe to bind introduced changed sequences in the repair template. Thus, the binding of FAM suggests the repair template has been successfully incorporated into the genome by HDR (Figure 19). Conversely, FAM-/HEX+ populations did not have incorporation of the FAM-probe specific sequence into the DNA.

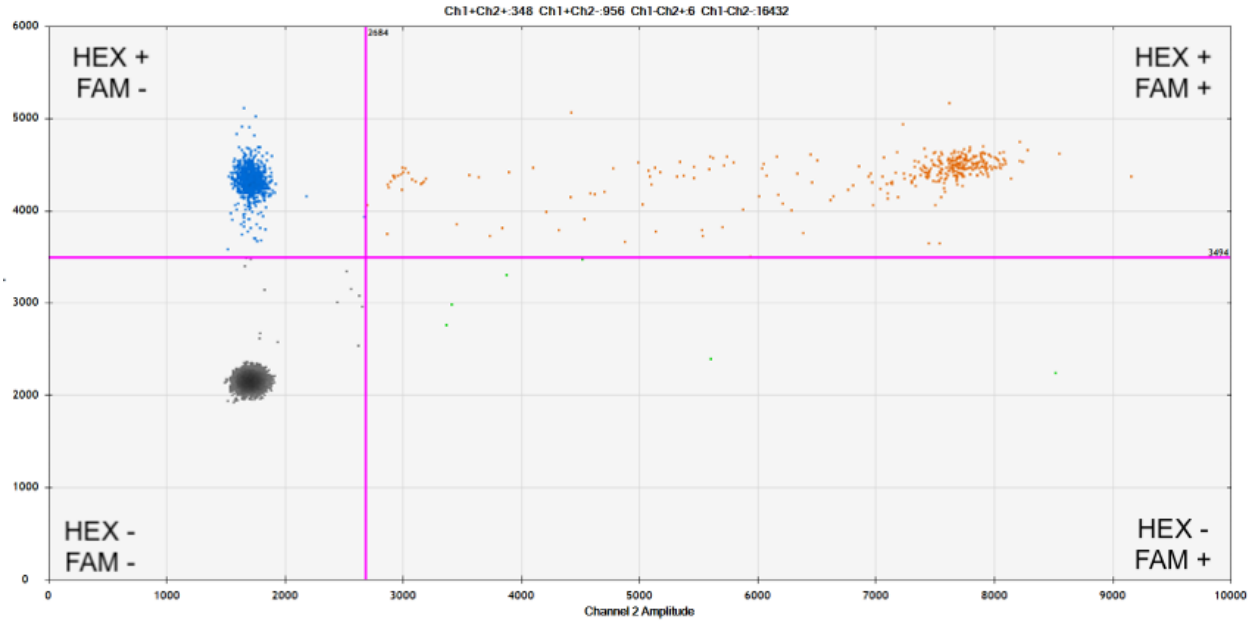

Figure 19. HDR gating electroporated fibroblast with i53 HDR enhancer

The plot shows a two-dimensional cluster in which channel 1amplitude fluorescence (FAM-HDR) is plotted against channel 2 amplitude (HEX). Plot is divided into four compartments. In the HEX+/FAM- population (top left box, blue dots), the reference DNA-binding HEX-labeled probe had bound while the repair template-binding FAM-HDR probe had not, indicating HDR events had not occurred. The HEX+/FAM+ population (top right box, orange dots) had bound both the general DNA-binding HEX-labeled probe and the repair template-binding FAM-labeled probe, indicating HDR events had occurred. The HEX-/FAM- population (bottom left box, grey dots) indicated no probes had attached to the DNA. The HEX-/FAM+ population (bottom right box, green dots) had bound the repair template-binding FAM-HDR probe but not the general DNA-binding HEX-labeled probe and is an unspecific binding during ddPCR.

Data from ddPCR titration experiments were statistically analyzed, enabling comparison of HDR enhancer efficiency at the various concentrations. The different concentrations of HDR enhancers were compared to the three controls; 1000ng EGFP mRNA, which was used as a control to check for interference in the RNP complex, RNP without any mRNA, and Mock. Mock cells were un-transfected fibroblasts that had been electroporated and were used to check for experimental toxicity in response to electroporation and as a control unedited sample for ddPCR analysis.

Results from titration experiments testing Ad5 showed that the HDR enhancer did not reduce the amount of NHEJ events below the RNP level. We observed no significant difference in the percentage of NHEJ events between the concentrations of Ad5. However, we saw a modest

increase of NHEJ at all concentrations except 2000ng, which was at the same level as the RNP control (Figure 20A). Additionally, no significant difference in the amount of HDR events happening at the various concentrations of Ad5 compared to RNP alone was observed. However, the HDR events were slightly reduced at all concentrations of Ad5 compared to the RNP control without statistical significance (Figure 20B).

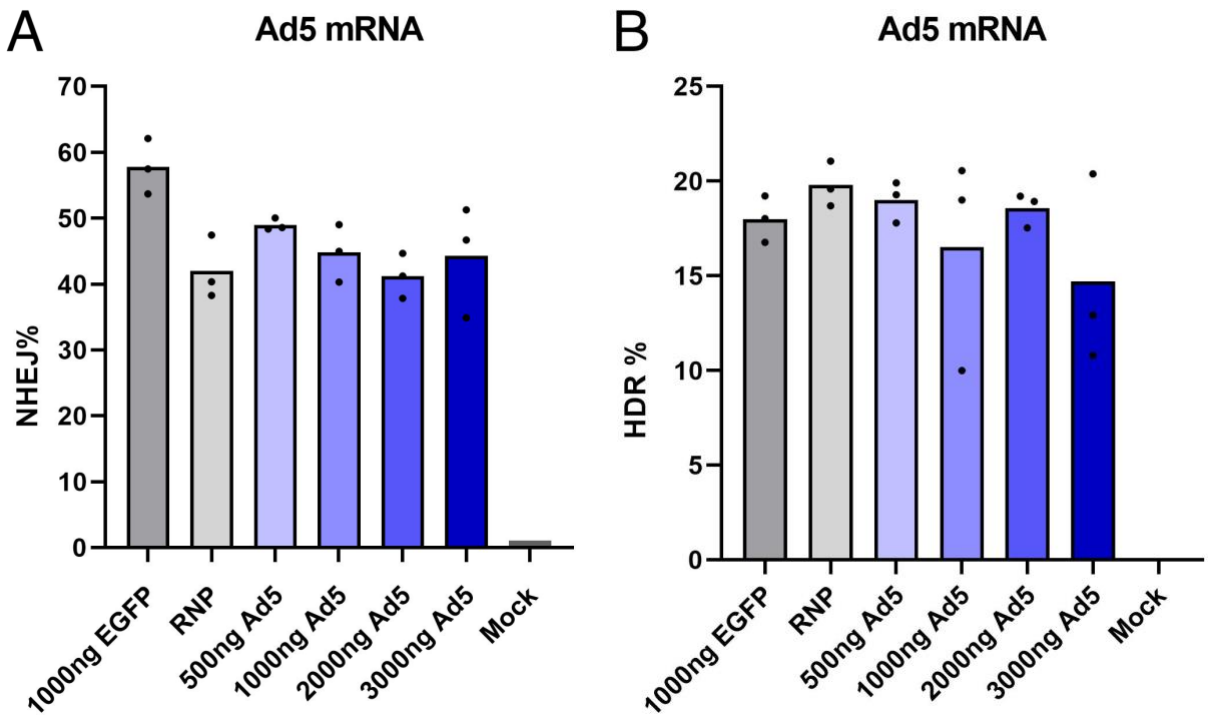

Figure 20. Editing efficiency in healthy donor fibroblasts with titration of HDR enhancer Ad5. *Electroporated fibroblast with Cas9 YY protein, ADA2 sgRNA WT3, HDR forward repair template, and Ad5 mRNA. Measuring NHEJ and HDR editing was done by ddPCR. Bar shows mean value, n = 3. Unpaired t-test against RNP revealed non-significant for all the data from NEHJ and HDR. NHEJ P-values 500ng = 0.0686, 1000ng = 0.5039, 2000ng = 0.8269, and 3000ng = 0.7086. HDR P-values 500ng = 0.4461, 1000ng = 0.3869, 2000ng = 0.2283, and 3000ng = 0.1643. Fibroblast donor (C27-1)*

Titration experiments testing the GSE56 HDR enhancer showed a significant increase in NHEJ events at all concentrations (Figure 21A). The two lowest concentrations of GSE56, 500ng, and 1000ng, had greater significance than the higher concentrations of GSE56, which were 2000ng and 3000ng. We observed no significant change in the amount of HDR events occurring at the different concentrations of HDR enhancers compared to RNP. However, an average increase of

approximately 7% points in HDR events occurred at 1000ng and 3000ng GSE56 (Figure 21B). The individual values were highly variable, which can explain why there was no significance in the increasement of HDR events.

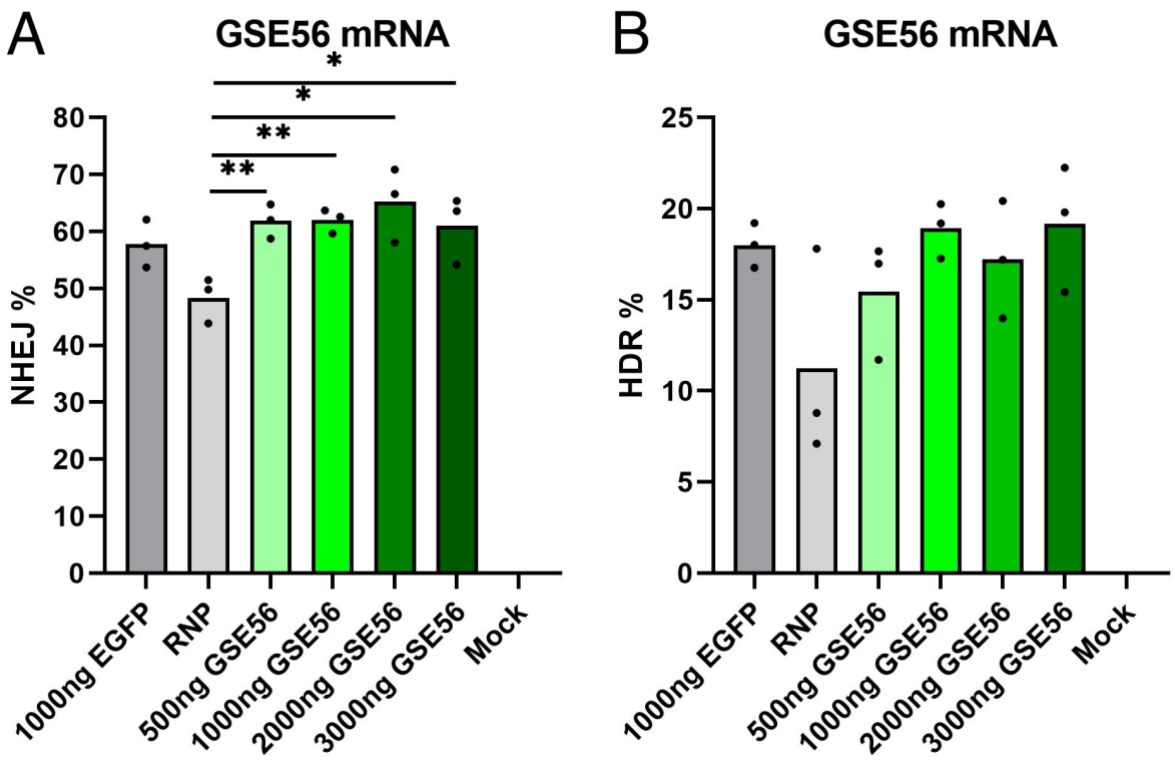

Figure 21. Editing levels of healthy donor fibroblasts with titration of HDR enhancer GSE56. *Electroporated fibroblast with Cas9 YY protein, ADA2 sgRNA WT3, HDR forward repair template, and GSE56 mRNA. Measuring NHEJ and HDR editing was done by ddPCR. Bar shows mean value, n = 3. Unpaired t-test against RNP revealed all data in NHEJ were significant with P-values 500ng = 0.0097, 1000ng = 0.0065, 2000ng = 0.0191, and 3000ng = 0.0389. Unpaired t-test against RNP revealed all data of HDR to be non-significant with P-values 500ng = 0.3312, 1000ng = 0.0893, 2000ng = 0.1919, and 3000ng = 0.1106. Fibroblast donor (C27-1)*

Titration experiments testing the i53 HDR enhancer showed no significant difference in the events of NHEJ compared to the RNP level. Although, there was some reduction in NHEJ events at 1000ng and 2000ng (Figure 22A). Even though the amount of NHEJ events stayed consistent at the different concentrations, there was a significant reduction in the number of HDR events that occurred at 2000ng and 3000ng of i53 mRNA (Figure 22B). 500ng mRNA was the only concentration barely increasing HDR events compared to RNP, however insignificant.

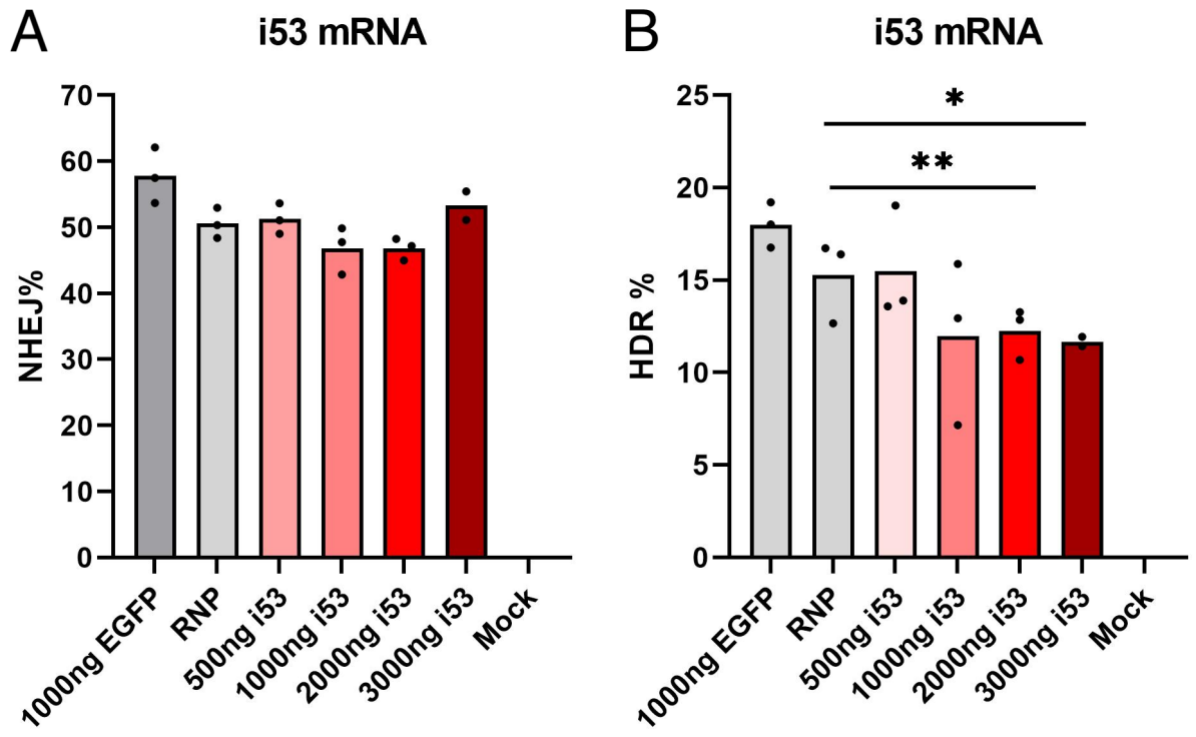

Figure 22. Editing levels of healthy donor fibroblasts with titration of HDR enhancer i53. *Electroporated fibroblast with Cas9 YY protein, ADA2 gRNA WT3, HDR forward repair template, and i53 mRNA. Measuring NHEJ and HDR editing was done by ddPCR. Bar shows mean value, n = 3 except 3000ng which had n = 2. Unpaired t-test against RNP revealed non-significant data for NHEJ with P-values 500ng = 0.4772, 1000ng = 0.4327, 2000ng = 0.3216, and 3000ng = 0.4839. For HDR Unpaired t-test against RNP revealed significance for 2000ng and 3000ng, but not for the rest of the data. HDR P-values 500ng = 0.2258, 1000ng= 0.0793, 2000ng = 0.0070, and 3000ng = 0.0576. Fibroblast donor (C27-1)*

Titration experiments testing the CYREN and Cry1 HDR enhancers did not result in a significant change in NHEJ events compared to the RNP level, although there was a slight increase in the percentage of NHEJ events in fibroblasts transfected with the Cry1 variant Cry1 WO NLS (Figure 23A). The amount of HDR events was reduced significantly below the RNP level by CYREN and all Cry1 variations. The reduction in HDR events that resulted from Cry1 was of greater significance than CYREN (Figure 23B)

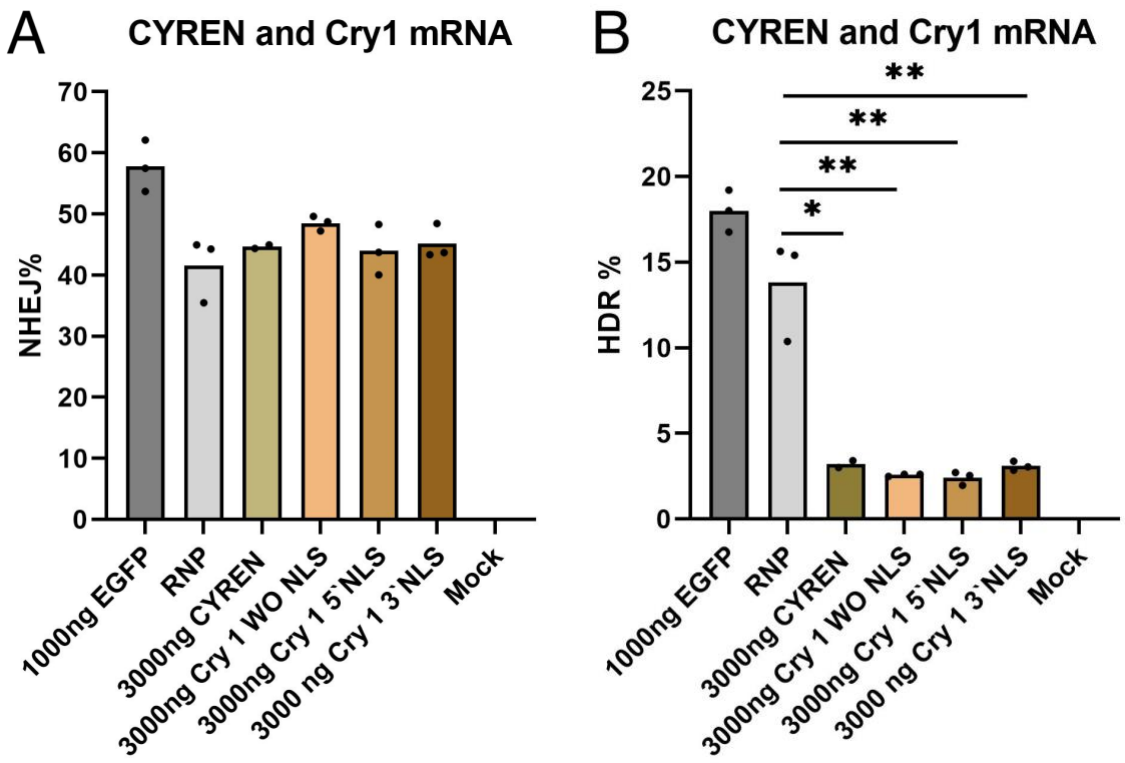

Figure 23. Editing levels of healthy donor fibroblasts with HDR enhancers CYREN and Cry1. *Electroporated fibroblast with Cas9 YY protein, ADA2 sgRNA WT3, HDR forward repair template, CYREN or Cry1 variants mRNA. Measuring NHEJ and HDR editing was done by ddPCR. Bar shows mean value, n = 3 except CYREN, which had n = 2. A) Unpaired t-test against RNP for NHEJ revealed non-significant data with P-values CYREN = 0.4814, Cry1 WO NLS = 0.0898, Cry1 5´end NLS = 0.5583, and Cry1 3´end NLS = 0.3552. B) Unpaired t-test against RNP revealed statical significant could be seen in all data of HDR with P-values CYREN = 0.0045, Cry1 WO NLS = 0.0028, Cry1 5´end NLS = 0.0028, and Cry1 3´end NLS = 0.0034. Fibroblast donor (C27-1)*

Our data suggest that none of the tested HDR enhancers: Ad5, GSE56, i53, CYREN, and Cry1 (all three variants) enhance the events of HDR when transfected into healthy donor fibroblasts singularly. Thus, none are preferable HDR enhancers for single use in transfected fibroblasts.

3.2.4 Testing Combinations of HDR Enhancers in Fibroblasts

After observing that each HDR enhancer alone had no positive effect on HDR, we wanted to test for possible synergic effects by combining several of these HDR enhancers. The titration experiment revealed that CYREN and Cry1 had the least HDR editing. These enhancers were therefore not included in the combination experiment. In addition, i53 got modified by adding a Flag tag on the end for increased mRNA stability. We tested 1000ng of i53Flag alone and investigated if it would perform better than i53 alone.

Compared to RNP, there was a significant increase in the percentage of NHEJ events happening in the presence of i53Flag + GSE56, GSE56 + Ad5, and i53Flag + Ad5 + GSE56. i53Flag and i53Flag + Ad5 performed better than the other HDR-enhancer combinations, as there were fewer events of NHEJ in their presence. However, i53Flag was the only HDR enhancer to reduce the percentage of NHEJ to below the RNP level. Although the observed reduction was minimal and insignificant (Figure 24A). i53Flag and i53Flag + Ad5 significantly decreased the amount of HDR events. The percentage of HDR events was not increased above the RNP level in cells transfected with any of the HDR-enhancer combinations but stayed consistent in all combinations containing GSE56 (Figure 24B).

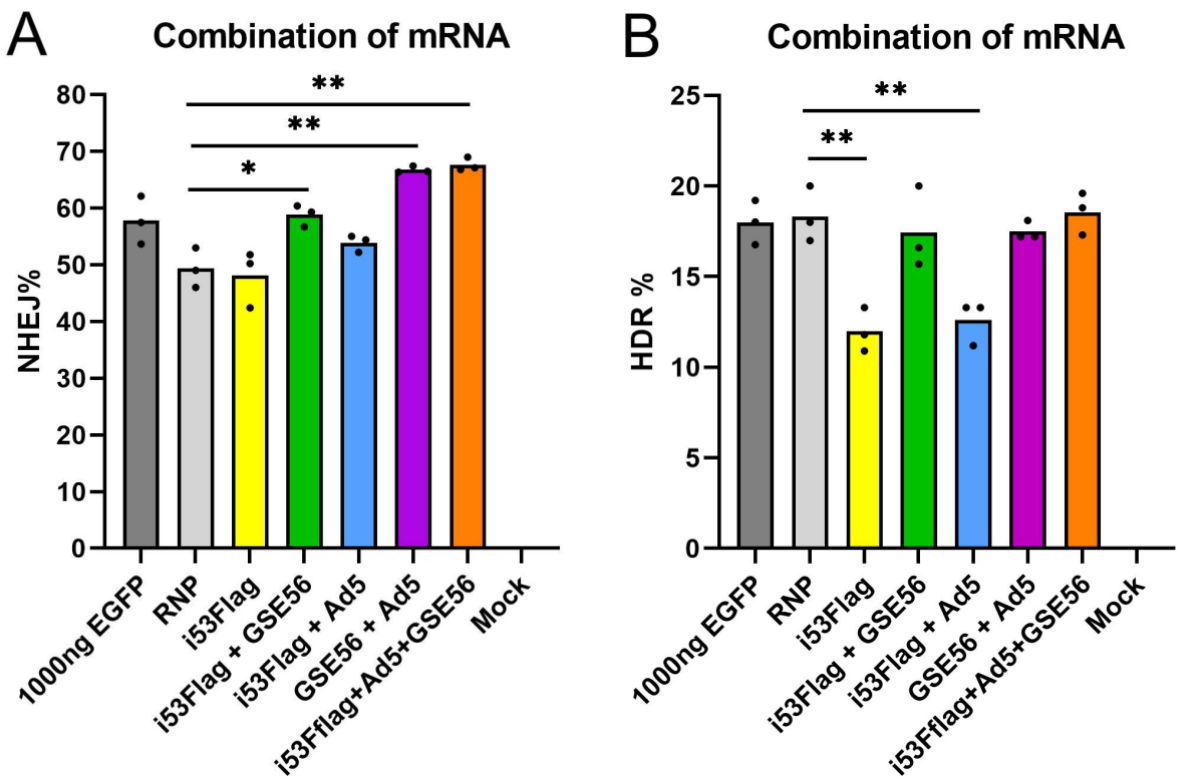

Figure 24. Editing levels of healthy donor fibroblasts with HDR enhancers tested together. *Electroporated fibroblasts with Cas9 YY protein, ADA2 sgRNA WT3, HDR forward repair template, and HDR enhancers mRNA. Measuring NHEJ and HDR editing was done by ddPCR. Bar shows mean value, n = 3. The concentration of each HDR enhancers was 1000ng. In NHEJ, unpaired t-test against RNP revealed statical significance in GSE56 + Ad5, GSE56 + Ad5 and in i53 Flag + Ad5 + GSE56. NHEJ P-values i53Flag = 0.7518, i53Flag + GSE56 = 0.0148, i53Flag + Ad5 = 0.1083, GSE56 + Ad5 = 0.0011, and i53Flag + Ad5 + GSE56 = 0.0010. B) For HDR, unpaired t-test against RNP revealed statical significance in i53 flag and I53 flag +Ad5. HDR P-values i53Flag = 0.0049, i53Flag + GSE56 = 0.5991, i53Flag + Ad5 = 0.0070, GSE56 + Ad5 = 0.4216, and i53Flag + Ad5 + GSE56 = 0,8438. Fibroblast donor (C27-1)*

4. Discussion

4.1 High Mortality Rate in Humanized Mice

8-9 weeks old NSG mice were irradiated and injected intravenously with edited and unedited local donor or commercial bought (AllCells) HSPCs. 60% of the mice involved in the experiment did not survive until the experimental end date. Extensive treatment using irradiation, risk of failed engraftment, stress-causing overhandling, and sudden food pellet change might have been factors contributing to high mortality, which is the first topic to be discussed.

Injecting HSC into SCID mice allowed simulating the development and function of a human immune system. Even though the mice were lacking an immune defense, it was possible the immune system still has some immune cells left (especially NK cells) to defend against the transplanted cells. Therefore, irradiation or chemotherapy is necessary to achieve myeloablation, the suppression of activity in the bone marrow in advance of transplantation [65].

The experimental end date was set to 16 weeks post-irradiation, but due to the major loss of mice, the experiment was forced to end at week 12. The experiment would have benefitted from proceeding through the last four weeks for ideal engraftment results. Nevertheless, 12 weeks is the earliest time to terminate the experiments, and studies recently showed survival and high engraftment even at week 18-20 [66] [67].

We weighted the mice every day for the first four weeks post-irradiation. Mice can experience up to 25% weight loss after irradiation but usually recover within three weeks [68]. A trend was observed as every single mouse lost 10%-13% of their baseline weight (2-4 g). Most mice regained the weight around week 3 (Figure 9), after being given acidic water as an antibiotic-free alternative and recovery gel. The mice in the control group were not irradiated and therefore were not expected to drop the same amount of weight as the irradiated mice. They did however lose some weight (<5% of body weight) due to stress from PBS injection and handling during the weighing. If a mouse would die in the first three weeks post-irradiation, we assumed the mouse either died of irradiation sickness or failed engraftment. NSG mice are known for being sensitive towards irradiation. Irradiation can increase morbidity, mortality, and cause distress which also can affect the engraftment results [69].

The entire treatment group 1A and seven out of nine mice in treatment group 3A died before week three (Figure 9A and D), which indicates the mice struggled with irradiation sickness. This was a surprising finding because mice within these groups received unedited HSC that did not show failed engraftment in the previously conducted pilot study (results not shown, conducted prior to master thesis) The mice got ordinary water until the day of irradiation. We believe the mice should have been given acidic water the last two-three days leading up to irradiation to get used to it. This could perhaps have reduced the number of deaths that occurred within the first three weeks of the experiment. Moreover, immunodeficient mice are prone to infection even from their own gut microbiota and it is common to observe opportunistic infections within individuals or even cages [70].

The recovery gel is a nutritionally fortified water gel that hydrates and supports the recovery of the mice. In some cages the recovery gel was popular, but it was difficult to keep control of which of the mice were eating it and which did not. In addition to acidic water in the water bottle, the mice got food pellets soaked in acidic water to increase the intake of nutrition. In the pilot mice study performed prior to the master thesis mouse experiment, mice were fond of the acidic water-soaked pellets. However, the animal facility changed the type of pellets without notifying us prior to the start of the thesis experiment. The new type of pellet (RM3) was rod-shaped and far denser than the previously rounded ball pellets (RM1). RM3 pellets did not swell as much as RM1 and were easily dissolved. We found a leftover batch of the RM1 pellets in week 4 and fed it to the mice to observe if they favored RM1 over RM3. Mice immediately ate the RM1 pellets soaked in acidic water, and clearly favored them over RM3 pellets. It was easier to keep track of the amount of the RM1 that had been eaten since we could count how many pellets were left in the cage. RM3 pellets, on the other hand, were observed as a wet pile, and often seemed to be untouched by the mice. RM1 pellets were fed to mice in bad shape to help them recover but could not be provided for all since the supply was limited.

Eight weeks after irradiation we managed to buy a stock of the RM1 pellets, which lead to increased weight and improved health for most of the mice. This was not documented, as mice only were routinely weighted the first four weeks after irradiation unless we suspected they were in poor shape (Figure 9). Although the mice were fed with RM1 pellets and many ate well

compared to before, mice seeming to recover died unexpectedly. Some of these mice were dissected to look for abnormalities (tooth cavities, stomach, and intestine obstruction, enlarged and spotty liver, signs of diarrhea). No abnormalities were observed during dissection and no mice seemed to have problems with overgrown teeth that potentially could inhibit eating. Additionally, the animal facility did not register any form of bacterial infection or virus outbreak in the period of the experiment. Thus, we believe the RM1 food pellets were provided too late for the mice to recover. Having the RM1 pellet type from the start could have helped the mice recover faster from irradiation and made them more robust by weight gain so that more mice could have survived. Better conditions and healthier mice could have provided more successful human engraftment results and allowed the experiment to last through all the 16 intended weeks.

4.2 Varying HSPC Engraftment Results

Mice reaching the humane endpoint were euthanized by cervical dislocation. Bones, spleen, and peripheral blood were collected. The cells extracted from these tissues were analyzed by flow cytometry to evaluate the level of human engraftment in each mouse.

Cell counting and viability of bone marrow and spleen-derived cells were checked after mice were sacrificed. Spleen cells proved to be less viable than bone marrow cells (Figure 11). We believe this was caused by extensive and harsh handling of the spleen cells. While the bone marrow cells were extracted by centrifugation of the bones, spleen cells were extracted by mashing the spleen through two sets of mesh filters. The mashing might have been too vigorous and can have affected the cell viability. Cell count of both spleen and bone marrow-derived cells went through red blood cell lysis to remove mice erythrocyte. The variations in number can have been caused by preserved red blood cells or by cell debris interfering with the count. We followed the centrifugation method for collecting bone marrow, instead of the golden standard of flushing the bones with PBS using a syringe [59]. This allowed us to collect bone marrow much faster and logistically easier.

Bone marrow, spleen, and peripheral blood-derived cells were subjected to flow cytometry, and all were gated in the same manner to identify human cells (Figure 12-15). The highest percentage of human engraftment was found in the bone marrow and the lowest in the peripheral blood. This finding was in line with what we expected since our NSG model does not provide the best

environmental conditions for HSC survival at the periphery nor survival of differentiated human myeloid cells and B- cells. In addition, the blood collection proved to be challenging and the collected volume of blood differed between the individual mice.

We choose to do flow cytometry on bone marrow-derived cells twice using two different sets of human and mouse markers, referred to as panel 1 and panel 2. One reason for doing this was to have a double validation of the human engraftment [60]. Gating of panel 2-stained BM cells resulted in a higher number of both mice cells and engrafted human cells compared to that of panel 1-stained BM cell gating (Figure 14). Panel 1 included two human marker binding antibodies (CD45 and HLA-A,B,C) and two mouse marker binding antibodies (mCD45.1 and mTER119), while panel 2 included only one human marker binding and mouse binding antibody (hCD45 and mCD45.1, respectively). We observed that panel 1 was more precise but required a flow cytometer with more complex settings and with more lasers than ours. Although panel 2 contained more antibodies than panel 1, panel 2 can be used in less advanced flow cytometers, such as our own FACS instrument (Sony SH800S cell sorter), and on occasions where we want to quickly check human engraftment levels (e.g., from sick mice).

Generally, HSC is part of the population of CD34+ cells, which is called hematopoietic stem and progenitor cells (HSPCs). Given a fact that we did not inject only pure LT-HSC or ST-HSC but rather a mix of different HSCs and progenitor cells, our observed engraftment could be affected by starting ratios between these progenitors and true HSC [71]. We saw varying results of human engraftment. Treatment group 2B had the highest percentage of human engraftment in bone marrow, spleen, and peripheral blood while treatment group 2A had the lowest human engraftment in all. Treatment group 2B had a 67 % mean of human engraftment in bone marrow, while treatment group 2A had a mean of 33%. Treatment groups 3A and 3B showed similar human engraftment results as treatment group 2B in bone marrow but lower human engraftment in spleen and peripheral blood. Interestingly, mice that received HSPCs from local donors performed as well as the commercial ones suggesting local cord blood donation can supply the needs of future *in vivo* experiments. The observed variations in human engraftment between the individuals indicate individual differences possibly can affect the level of engraftments, such as stress, to what degree their health was compromised by irradiation, and appetite. Varying engraftment results in

individuals of the same strain are not unique to our experiment and have been observed in other studies as well. A gene knock-in study by Willinger et al showed HSPC engraftment varied from 5-50% in blood, 15-70% in the spleen, and 40-80% in the bone marrow [72]. In another study, HSC engraftment results ranged between 20-90% in week 12 and between 40-78% in week 18 [73].

Human engraftment results in the peripheral blood were the most variable (figure 16A). Collecting blood after cervical dislocation is challenging, as separating the spinal cord from the head can result in a rapture of the main artery if not performed with precision. It takes approximately 1 minute from cervical dislocation until the mouse is opened and blood can be collected by heart puncture. The preferable way to collect blood is by heart puncture prior to cervical dislocation, where the mouse is under anesthesia and the heart is still pumping blood and the mouse is alive. This is an advanced method that makes it possible to collect higher amounts of blood (1-1.5mL). However, if sedated incorrectly, it could cause unnecessary suffering for the mouse and could be very stressful for the researcher. Since the experiment had to come to an early end, we did not have enough time to practice this technique. Collection of blood was therefore performed after euthanasia by cervical dislocation. Therefore, the amount of blood we were able to collect from each mouse was spare, ranging between 0.1-0.5mL. Thus, the number of cells to analyze by flow cytometry was very low, often less than 5,000 cells, and could compromise the true engraftment levels in the periphery mouse environment.

4.3 Single HDR Enhancers Did Not Promote HDR

Various HDR enhancers were tested in fibroblasts with the goal to optimize precise genome editing for ADA2 locus. We evaluated how both single-use and combinations of these HDR enhancers would affect the number of HDR events, which is associated with precise gene editing. To do this, DNA sequences of HDR enhancers were cloned into IVT-optimal plasmid backbone, and mRNA was produced by IVT. An RNP complex, ssODN repair template together with HDR enhancer mRNAs were delivered to healthy donor fibroblast cells by electroporation. Cells were collected 4 days later and ddPCR was performed to confirm editing outcomes.

IVT is an advanced technique that requires an RNase-free environment to produce clean mRNA and failed IVT is often discovered at the last step of the protocol (Figure 17C). In general, we observed all the mRNAs produced were high in quality and quantity. mRNA concentrations were higher than 800 ng/µL, which was sufficient for electroporation experiments.

When we tested each HDR enhancer individually in fibroblast, no major reduction in NHEJ events was observed. i53 was the only HDR enhancer to reduce the percentage of NHEJ events below the level of the RNP control. Cells edited using 1000 ng and 2000 ng of i53 mRNA had a mean of 46.8% NHEJ events, barely below that of RNP, which was 50.5% (Figure 22A). This was insignificant and not enough change had occurred to conclude improvements were observed. 1000ng and 2000ng i53 mRNA had a mean of 12% HDR events compared to 15% from RNP (Figure 22B). Contradictory to our results, there have been studies showing i53 mRNA used in HSPCs resulted in a 1.5-fold increase of HDR events [74]. In this study, they used up to 48 pmol of i53 mRNA in HPSCs which may have a cell-specific effect.

Ad5 has been found to increase editing efficiencies in human HSCP by activating the E2F transcriptional pathway and transiently activating CDK2 inducing the S/G2 cell cycle phase [61]. Results from our ddPCR experiments in fibroblast were not in line with this finding in HSPC, as most concentrations of Ad5 increased the events of NHEJ and reduced the events of HDR (Figure 20A-B).

CYREN and Cry1 variants were tested only at 3000ng and not titrated as the other HDR enhancers. The amount of NHEJ events was comparable to RNP. Interestingly, CYREN and CRY1 variants reduced the percentage of HDR events significantly below the RNP level, with a mean of 3% HDR for each of them (Figure 23B). It is possible the high concentration of mRNA was toxic to the cells, which resulted in the downregulation of HDR events. Therefore, it would be interesting to test Cry1 and CYREN at a lower concentration to see if that could increase HDR. CRY1 is a known coregulator of the circadian rhythm and recent findings suggest Cry1 is associated with homologues recombination regulation mediated to DNA damage response (DDR), which contradicts our results [63]. On the other hand, it has been shown in a cancer-specific environment.

There are ongoing debates regarding the function of CYREN. CYREN could be a positive regulator of NHEJ or promote HDR since it binds and protect the DNA break overhang [62].

4.4 Combinations of HDR Enhancers Did Not Promote HDR

Results using HDR enhancer mRNA alone were not promising since interestingly, most HDR enhancers did not enhance HDR. We combined HDR enhancers to see if it would increase tilt the balance between NHEJ and HDR. Due to the low percentage of HDR events using CYREN and Cry1 variants, these HDR enhancers were omitted from combination experiments. Ad5, GSE56, and i53 mRNAs were used for the experiments, however, a Flag was added to i53 to increase the stability. i53Flag mRNA was tested alone at 1000ng but did not increase the HDR events compared to i53 condition. Like for single HDR enhancer experiments, the NHEJ events were not reduced below the RNP level but rather increased when combining HDR enhancers (Figure 24A). All combinations except i53Flag and i53Flag+Ad5 resulted in a significant increase in NHEJ events.

The HDR enhancer combinations of i53Flag + GSE56 + AD5 had the highest level of HDR events, with a mean of 18.5%, barely above RNP level which had a mean of 18.3% (Figure 24B). Our result did not show increased HDR events when using i53Flag mRNA, but rather reduced the HDR events at the higher concentrations, which could suggest toxicity at increasing concentrations. In a study using the HEK293T cell line, a 1.3-fold increase in HDR event was observed when inhibiting 53BP1 with i53Flag [75].

In the presence of GSE56 mRNA, the percentage of HDR events was comparable to that of RNP mRNA (Figure 24B). All combinations excluding GSE56 had HDR levels below RNP. Thus, results could indicate that GSE56 had a compensatory effect in combination experiments where other enhancers act to suppress HDR events. In our results, HDR events in cells electroporated with Ad5 mRNA alone were below RNP (Figure 20B). Neither did the presence of Ad5 in combination experiments favor HDR events. Ad5 is involved in the E2F transcriptional pathway which forces the cell into S/G2 cycle phase helping the HDR pathway, which suggests we should have observed an increase in the HDR compartment in our results. In a study performed with HSPC, Ad5 mRNA was found to increase the HDR events. Combining Ad5 with GSE56 mRNA

further elevated the HDR to a mean of 50% in therapeutically relevant long-term HSC. Surprisingly, GSE56 mRNA alone did not increase the HDR in this study with the fibroblast [61].

The HDR enhancers Ad5, GSE56, i53, i53Flag, CYREN, and Cry1 variants were tested in healthy donor fibroblast. As far as we know this has not been tested before in fibroblast with ssODN repair template. From our observation delivery of RNP complexes was with HDR enhancer mRNA alone or as a combination not improving HDR in this type of primary cells. Compared to NHEJ, HDR is a slow process and takes 7 hours or more to complete the repair pathway [76]. It could be that HDR enhancers are inhibiting the NHEJ pathway but not long enough time for HDR to complete the HDR repair pathway. Also, an idea could be to try protein delivery of the HDR enhancers as an alternative to mRNA delivery, to see if that could have some effect in increasing HDR events since mRNA can trigger immune signaling inside the cells and is not timed properly together with the RNPs active window [77]. Ultimately, screening of the HDR enhancers should be done with AAV repair template as an alternative to ssODN since all the HDR enhancers were tested together with AAV strategy.

5. Conclusion

To conclude, our mice experiment has demonstrated successful human engraftment 12 weeks after intravenous injection of HSPC. Mice achieved high human engraftment in bone marrow, where edited cells engrafted better than unedited HSCP. The spleen and peripheral blood had lower and more variation in the human engraftment. We observed an unexpectedly high number of death (60%) which we believe is connected to irradiation sickness, failed engraftment or change of eating habits. We have also demonstrated that two different FACS panels can be used to measure human engraftment on a different flow cytometer in comparable way. We observed valuable information about the effect of the conditioning regiment and HSPCs donor to donor variability which will be helpful for further experiments involving mice.

Additionally, we wanted to favor the HDR pathway in healthy donor fibroblasts with previously published HDR enhancers. We used Ad5, Cry 1 variants, CYREN, GSE56, and i53 (including i53 Flag) as a mRNA format, which revealed no increase in HDR when using them individually. Neither did the HDR enhancer mRNA reduce NHEJ. With inspiration from other studies, we combined HDR enhancers to investigate whether that would elevate the HDR events. We employed different combinations with 1000ng of Ad5, GSE56, and i53Flag mRNA. None of the HDR-enhancer combinations promoted HDR nor reduced NHEJ in fibroblasts.

In conclusion, more experiments are needed in order to gain knowledge and optimize gene editing to be utilized in the treatment of monogenic childhood immune diseases.

6. Future perspectives

For future mice studies, we plan to replicate the human engraftment experiments with DADA2-patient bone marrow-derived HSPCs. In parallel, it would be very informative and useful to test the engraftment of human HSPCs in the mouse strain that does not require any myeloablation steps (chemically or by irradiation). Next, we would like to expand the loci of interest to other clinically relevant diseases as well as test feasibility, efficiency, and safety.

Although all HDR enhancer mRNA used in this master thesis has been reported to promote HDR in other cell lines or HSPCs, none was revealed to be effective in favoring the HDR repair pathway over NHEJ in fibroblasts. Therefore, we have to investigate other options for HDR promotion in fibroblasts in the future. By delivering the HDR enhancers directly as proteins rather than mRNA, we could achieve a more stable therapeutic strategy by avoiding possible pitfalls involved in mRNA translation issues and stability concerns within the cells. If the protein-based therapeutics reveal the HDR enhancers to have HDR promoting effects in fibroblasts, the next step will be to test the HDR enhancers in other primary cells, such as HSC/HSCPS and peripheral blood and mononuclear cells (PBMCs). If this also is successful, it allows for improved gene-editing techniques, which subsequentially can be utilized in future mice experiments and, ideally, eventually in clinical setup.

7. References

1. Piel, F.B., M.H. Steinberg, and D.C. Rees, *Sickle Cell Disease.* New England Journal of Medicine, 2017. **376**(16): p. 1561-1573.
2. Hoffman, R., *Hematology : basic principles and practice*. 6th ed. 2013, Philadelphia, PA: Saunders/Elsevier. xxxi, 2343 p.
3. Seita, J. and I.L. Weissman, *Hematopoietic stem cell: self?renewal versus differentiation*. 2010: Hoboken, NJ :. p. 640-653.
4. Wilson, A. and A. Trumpp, *Bone-marrow haematopoietic-stem-cell niches.* Nature Reviews Immunology, 2006. **6**(2): p. 93-106.
5. Ito, K. and Paul, *HSC Contribution in Making Steady-State Blood.* Immunity, 2016. **45**(3): p. 464-466.
6. Lam, W.Y. and D. Bhattacharya, *Metabolic Links between Plasma Cell Survival, Secretion, and Stress.* Trends in Immunology, 2018. **39**(1): p. 19-27.
7. Abbas, A.K., et al., *Cellular and molecular immunology*. Ninth edition. ed. 2018, Philadelphia, PA: Elsevier. x, 565 pages.
8. Bonilla, F.A. and H.C. Oettgen, *Adaptive immunity.* Journal of Allergy and Clinical Immunology, 2010. **125**(2): p. S33-S40.
9. Forthal, D.N., *Functions of Antibodies.* Microbiol Spectr, 2014. **2**(4): p. AID-0019-2014.
10. Kondělková, K., et al., *Regulatory T cells (Treg) and Their Roles in Immune System with Respect to Immunopathological Disorders.* Acta Medica (Hradec Kralove, Czech Republic), 2010. **53**(2): p. 73-77.
11. Cirillo, E., et al., *Severe combined immunodeficiency--an update.* Ann N Y Acad Sci, 2015. **1356**: p. 90-106.
12. Meyts, I. and I. Aksentijevich, *Deficiency of Adenosine Deaminase 2 (DADA2): Updates on the Phenotype, Genetics, Pathogenesis, and Treatment.* J Clin Immunol, 2018. **38**(5): p. 569-578.
13. Hong, Y., et al., *Lentiviral Mediated ADA2 Gene Transfer Corrects the Defects Associated With Deficiency of Adenosine Deaminase Type 2.* Frontiers in Immunology, 2022. **13**.
14. Giralt, S. and M.R. Bishop, *Principles and Overview of Allogeneic Hematopoietic Stem Cell Transplantation*. 2009, Springer US. p. 1-21.
15. Snowden, J.A., et al., *Autologous haematopoietic stem cell transplantation (aHSCT) for severe resistant autoimmune and inflammatory diseases – a guide for the generalist.* Clinical Medicine, 2018. **18**(4): p. 329-334.
16. Ball, L.M. and R.M. Egeler, *Acute GvHD: pathogenesis and classification.* Bone Marrow Transplantation, 2008. **41**(S2): p. S58-S64.
17. Park, M. and J.J. Seo, *Role of HLA in Hematopoietic Stem Cell Transplantation.* Bone Marrow Res, 2012. **2012**: p. 680841.
18. Sheldon, S. and K. Poulton, *HLA Typing and Its Influence on Organ Transplantation*. Humana Press. p. 157-174.
19. Nowak, J., *Role of HLA in hematopoietic SCT.* Bone Marrow Transplantation, 2008. **42**(S2): p. S71-S76.

20. Reddy, P. and J.L.M. Ferrara, *Mouse models of graft-versus-host disease*, in *StemBook*. 2008: Cambridge (MA).
21. Pearson, T., D.L. Greiner, and L.D. Shultz, *Humanized SCID Mouse Models for Biomedical Research*. 2008, Springer Berlin Heidelberg. p. 25-51.
22. McCune, J.M., et al., *The SCID-hu mouse: murine model for the analysis of human hematolymphoid differentiation and function.* Science, 1988. **241**(4873): p. 1632-9.
23. McCune, J., et al., *The SCID-hu mouse: a small animal model for HIV infection and pathogenesis.* Annu Rev Immunol, 1991. **9**: p. 399-429.
24. Marsden, M.D., *Benefits and limitations of humanized mice in HIV persistence studies.* Retrovirology, 2020. **17**(1).
25. Laboratory, J. *NOD.Cg-Prkdcscid Il2rgtm1Wjl/SzJ*. 2022 [cited 2022 12.05.2022]; Available from: https://www.jax.org/strain/005557.
26. Hickman, D.L., et al., *Commonly Used Animal Models*. 2017, Elsevier. p. 117-175.
27. Deroche-Gamonet, V., D. Belin, and P.V. Piazza, *Evidence for Addiction-like Behavior in the Rat.* Science, 2004. **305**(5686): p. 1014-1017.
28. Fan, J., et al., *Neural Activities in Multiple Rat Brain Regions in Lithium-Pilocarpine-Induced Status Epilepticus Model.* Frontiers in Molecular Neuroscience, 2020. **12**.
29. Bryda, E.C., *The Mighty Mouse: the impact of rodents on advances in biomedical research.* Mo Med, 2013. **110**(3): p. 207-11.
30. Hajar, R., *Animal testing and medicine.* Heart Views, 2011. **12**(1): p. 42.
31. Botting, J., *Animals and Medicine: The Contribution of Animal Experiments to the Control of Disease*. 2015: Open Book Publishers.
32. Somers, G.F., *THALIDOMIDE AND CONGENITAL ABNORMALITIES.* The Lancet, 1962. **279**(7235): p. 912-913.
33. Barré-Sinoussi, F. and X. Montagutelli, *Animal models are essential to biological research: issues and perspectives.* Future Science OA, 2015. **1**(4).
34. Chinwalla, A.T., et al., *Initial sequencing and comparative analysis of the mouse genome.* Nature, 2002. **420**(6915): p. 520-562.
35. McCouch, S.R., *Genomics and Synteny.* Plant Physiology, 2001. **125**(1): p. 152-155.
36. Vogel, A.B., et al., *BNT162b vaccines protect rhesus macaques from SARS-CoV-2.* Nature, 2021. **592**(7853): p. 283-289.
37. Commision, E. *Legislation for the protection of animals used for scientific purposes*. 05.05.2022]; Available from: https://ec.europa.eu/environment/chemicals/lab_animals/legislation_en.htm.
38. Gaul, H., *Mutations in plant breeding.* Radiation botany, 1964. **4**(3): p. 155,IN1,159,IN3,161,IN5,169,IN7,173,IN11,193,IN13,195-158,IN2,160,IN4,168,IN5,172,IN10,192,IN12,194,IN14,232.
39. Carroll, D., *Genome Editing: Past, Present, and Future.* Yale J Biol Med, 2017. **90**(4): p. 653-659.
40. Gaj, T., C.A. Gersbach, and C.F. Barbas, III, *ZFN, TALEN, and CRISPR/Cas-based methods for genome engineering.* Trends in Biotechnology, 2013. **31**(7): p. 397-405.
41. Jang, H.-K., et al., *Current trends in gene recovery mediated by the CRISPR-Cas system.* Experimental & Molecular Medicine, 2020. **52**(7): p. 1016-1027.

42. Nadakuduti, S.S., et al., *Evaluation of Methods to Assess in vivo Activity of Engineered Genome-Editing Nucleases in Protoplasts.* Front Plant Sci, 2019. **10**: p. 110.
43. Potter, H., *Transfection by Electroporation.* Current Protocols in Molecular Biology, 2003. **62**(1).
44. Bijlani, S., et al., *The Role of Recombinant AAV in Precise Genome Editing.* Front Genome Ed, 2021. **3**: p. 799722.
45. Klug, A., *The discovery of zinc fingers and their development for practical applications in gene regulation and genome manipulation.* Quarterly Reviews of Biophysics, 2010. **43**(1): p. 1-21.
46. Gaj, T., et al., *Genome-Editing Technologies: Principles and Applications.* Cold Spring Harbor Perspectives in Biology, 2016. **8**(12): p. a023754.
47. Gupta, R.M. and K. Musunuru, *Expanding the genetic editing tool kit: ZFNs, TALENs, and CRISPR-Cas9.* Journal of Clinical Investigation, 2014. **124**(10): p. 4154-4161.
48. Knott, G.J. and J.A. Doudna, *CRISPR-Cas guides the future of genetic engineering.* Science, 2018. **361**(6405): p. 866-869.
49. Jinek, M., et al., *A programmable dual-RNA-guided DNA endonuclease in adaptive bacterial immunity.* Science, 2012. **337**(6096): p. 816-21.
50. Doudna, J.A., *The promise and challenge of therapeutic genome editing.* Nature, 2020. **578**(7794): p. 229-236.
51. Makarova, K.S., et al., *Evolutionary classification of CRISPR–Cas systems: a burst of class 2 and derived variants.* Nature Reviews Microbiology, 2020. **18**(2): p. 67-83.
52. Ran, F.A., et al., *Genome engineering using the CRISPR-Cas9 system.* Nature Protocols, 2013. **8**(11): p. 2281-2308.
53. Zhang, H.-X., Y. Zhang, and H. Yin, *Genome Editing with mRNA Encoding ZFN, TALEN, and Cas9.* Molecular Therapy, 2019. **27**(4): p. 735-746.
54. Chen, H., J. Choi, and S. Bailey, *Cut Site Selection by the Two Nuclease Domains of the Cas9 RNA-guided Endonuclease.* Journal of Biological Chemistry, 2014. **289**(19): p. 13284-13294.
55. Vítor, A.C., et al., *Studying DNA Double-Strand Break Repair: An Ever-Growing Toolbox.* Frontiers in Molecular Biosciences, 2020. **7**.
56. Brault, J., et al., *CRISPR-targeted MAGT1 insertion restores XMEN patient hematopoietic stem cells and lymphocytes.* Blood, 2021. **138**(26): p. 2768-2780.
57. Abdelnour, S.A., et al., *The Potential of CRISPR/Cas9 Gene Editing as a Treatment Strategy for Inherited Diseases.* Frontiers in Cell and Developmental Biology, 2021. **9**.
58. Zhao, Z., et al., *Review of applications of CRISPR-Cas9 gene-editing technology in cancer research.* Biological Procedures Online, 2021. **23**(1).
59. Heib, T., et al., *Isolation of murine bone marrow by centrifugation or flushing for the analysis of hematopoietic cells – a comparative study.* Platelets, 2021. **32**(5): p. 601-607.
60. Bak, R.O., D.P. Dever, and M.H. Porteus, *CRISPR/Cas9 genome editing in human hematopoietic stem cells.* Nature Protocols, 2018. **13**(2): p. 358-376.
61. Ferrari, S., et al., *Efficient gene editing of human long-term hematopoietic stem cells validated by clonal tracking.* Nature Biotechnology, 2020. **38**(11): p. 1298-1308.
62. Arnoult, N., et al., *Regulation of DNA repair pathway choice in S and G2 phases by the NHEJ inhibitor CYREN.* Nature, 2017. **549**(7673): p. 548-552.

63. Shafi, A.A., et al., *The circadian cryptochrome, CRY1, is a pro-tumorigenic factor that rhythmically modulates DNA repair.* Nature Communications, 2021. **12**(1).
64. Lesueur, L.L., L.M. Mir, and F.M. André, *Overcoming the Specific Toxicity of Large Plasmids Electrotransfer in Primary Cells In Vitro.* Molecular Therapy - Nucleic Acids, 2016. **5**(3): p. e291.
65. Nomura, T., T. Watanabe, and S. Habu, *Humanized mice. Preface.* Curr Top Microbiol Immunol, 2008. **324**: p. v-vi.
66. Díaz De La Guardia, R., et al., *Engraftment characterization of risk-stratified AML in NSGS mice.* Blood Advances, 2021. **5**(23): p. 4842-4854.
67. Romero, Z., et al., *Editing the Sickle Cell Disease Mutation in Human Hematopoietic Stem Cells: Comparison of Endonucleases and Homologous Donor Templates.* Molecular Therapy, 2019. **27**(8): p. 1389-1406.
68. Duran-Struuck, R. and R.C. Dysko, *Principles of bone marrow transplantation (BMT): providing optimal veterinary and husbandry care to irradiated mice in BMT studies.* J Am Assoc Lab Anim Sci, 2009. **48**(1): p. 11-22.
69. Chadalavada, D., et al., *Irradiated compared with nonirradiated NSG mice for the development of a human B-cell lymphoma model.* Comp Med, 2014. **64**(3): p. 179-85.
70. Ragland, N.H., E.L. Miedel, and R.W. Engelman, *PCR Prevalence of Murine Opportunistic Microbes and their Mitigation by Using Vaporized Hydrogen Peroxide.* Journal of the American Association for Laboratory Animal Science, 2019. **58**(2): p. 208-215.
71. Naldini, L., *Genetic engineering of hematopoiesis: current stage of clinical translation and future perspectives.* EMBO Molecular Medicine, 2019. **11**(3): p. e9958.
72. Willinger, T., et al., *Improving human hemato-lymphoid-system mice by cytokine knock-in gene replacement.* Trends in Immunology, 2011. **32**(7): p. 321-327.
73. Hasgur, S., et al., *Generation of Immunodeficient Mice Bearing Human Immune Systems by the Engraftment of Hematopoietic Stem Cells*. 2016, Springer New York. p. 67-78.
74. Sweeney, C.L., et al., *Correction of X-CGD patient HSPCs by targeted CYBB cDNA insertion using CRISPR/Cas9 with 53BP1 inhibition for enhanced homology-directed repair.* Gene Therapy, 2021. **28**(6): p. 373-390.
75. Canny, M.D., et al., *Inhibition of 53BP1 favors homology-dependent DNA repair and increases CRISPR–Cas9 genome-editing efficiency.* Nature Biotechnology, 2018. **36**(1): p. 95-102.
76. Mao, Z., et al., *Comparison of nonhomologous end joining and homologous recombination in human cells.* DNA Repair, 2008. **7**(10): p. 1765-1771.
77. Piras, F. and A. Kajaste-Rudnitski, *Antiviral immunity and nucleic acid sensing in haematopoietic stem cell gene engineering.* Gene Therapy, 2021. **28**(1-2): p. 16-28.

Appendix A

Machines

- Automated Droplet Generator (Bio-Rad)
- QIAcube HT (QIAGEN)
- QX200™ Droplet Reader (Bio-Rad)
- Lonza 4D- nucleofector system (software 2.1).
- Heat sealer
- PCR machine (Bio-Rad)
- BD LSR II Flow cytometer
- BL-2 laminar hood
- Incubator

Material

- Falcon ® Round-Bottom Tube with cell strainer cap
- PBS (Homemade)
- QIAAmp 96 DNA kit (QIAGEN)
- QIAcube HT plasticware (QIAGEN)
- Reagent Trough (with lid) 70 & 170ml
- DG32™ Automated Droplet Generator Cartridges
- ddPCR Plates, 96 wells, Semi-Skirted (Bio-Rad)
- ddPCR™ Supermix for Probes (No dUTP) (Bio-Rad)
- Automated droplet generation oil for probes (Bio-Rad)
- 2 L (2 x 1 L), oil for use with droplet reader in the QX200™/QX100™ Droplet Digital™ PCR Systems (Bio-Rad)
- Armadillo High-Performance 96-Well PCR Plates (Thermo Fisher Scientific)
- Pierceable Foil Heat Seal (Bio-Rad)
- Nunc™ Aluminum Sealing Tape for 96 well plates (Thermo Fisher Scientific)
- RNAase away

Appendix B

HDR enhancer sequences

EGFP

5`

ATGGTGAGCAAGGGCGAGGAGCTGTTCACCGGGGTGGTGCCCATCCTGGTCGAGCTGGACGGCGACG
TAAACGGCCACAAGTTCAGCGTGTCCGGCGAGGGCGAGGGCGATGCCACCTACGGCAAGCTGACCCTG
AAGTTCATCTGCACCACCGGCAAGCTGCCCGTGCCCTGGCCCACCCTCGTGACCACCCTGACCTACGGCG
TGCAGTGCTTCAGCCGCTACCCCGACCACATGAAGCAGCACGACTTCTTCAAGTCCGCCATGCCCGAAG
GCTACGTCCAGGAGCGCACCATCTTCTTCAAGGACGACGGCAACTACAAGACCCGCGCCGAGGTGAAG
TTCGAGGGCGACACCCTGGTGAACCGCATCGAGCTGAAGGGCATCGACTTCAAGGAGGACGGCAACAT
CCTGGGGCACAAGCTGGAGTACAACTACAACAGCCACAACGTCTATATCATGGCCGACAAGCAGAAGA
ACGGCATCAAGGTGAACTTCAAGATCCGCCACAACATCGAGGACGGCAGCGTGCAGCTCGCCGACCACT
ACCAGCAGAACACCCCCATCGGCGACGGCCCCGTGCTGCTGCCCGACAACCACTACCTGAGCACCCAGT
CCGCCCTGAGCAAAGACCCCAACGAGAAGCGCGATCACATGGTCCTGCTGGAGTTCGTGACCGCCGCC
GGGATCACTCTCGGCATGGACGAGCTGTACAAG 3`

i53

5`

ATGTTGATTTTCGTGAAAACCCTTACCGGGAAAACCATCACCCTCGAGGTTGAACCCTCGGATACGATAG
AAAATGTAAAGGCCAAGATCCAGGATAAGGAAGGAATTCCTCCTGATCAGCAGAGACTGGCCTTTGCTG
GCAAATCGCTGGAAGATGGACGTACTTTGTCTGACTACAATATTCTAAAGGACTCTAAACTTCATCCTCT
GTTGAGACTTCGTTGA 3`

i53 Flag

5`

GACTACAAAGACGATGACGATAAAGCCGCCAGTTTAAACGGCGCGCCATTAATTAAGGATCCAATGTTG
ATTTTCGTGAAAACCCTTACCGGGAAAACCATCACCCTCGAGGTTGAACCCTCGGATACGATAGAAAAT
GTAAAGGCCAAGATCCAGGATAAGGAAGGAATTCCTCCTGATCAGCAGAGACTGGCCTTTGCTGGCAA

ATCGCTGGAAGATGGACGTACTTTGTCTGACTACAATATTCTAAAGGACTCTAAACTTCATCCTCTGTTGA
GACTTCGTTGA 3`

GSE56
5`
ATGGATGGATGGTGTCCTGGGAGAGACCGTCGGACAGAGGAAGAAAATTTCCGCAAAAAAGAAGAGC
ATTGCCCGGAGCTGCCCCCAGGGAGTGCAAAGAGAGCACTGCCCACCAGCACAAGCTCCTCTCCCCAGC
AAAAGAAAAAACCACTCGATGGAGAATATTTCACCCTTAAGATCCGTGGGCGTGAGCGCTTCGAGATGT
TCCGAGAGCTGAATGAGGCCTTGGAATTAAAGGATGCCCGTGCTGCCGAGGAGTCAGGAGACAGCAG
GGCTCACTCCAGCTACCCGAAGATAGTTAGTTAG 3`

Ad5 E4orf6/7
5`
ATGACTACGTCCGGCGTTCCATTTGGCATGACACTACGACCAACACGATCTCGGTTGTCTCGGCGCACTC
CGTACAGTAGGGATCGCCTACCTCCTTTTGAGACAGAGACCCGCGCTACCATACTGGAGGATCATCCGC
TGCTGCCCGAATGTAACACTTTGACAATGCACAACGCGTGGACTTCCCCTTCGCCGCCCGTTGAGCAACC
GCAAGTTGGACAGCAGCCTGTGGCTCAGCAGCTGGACAGCGACATGAACTTAAGCGAGCTGCCCGGGG
AGTTTATTAATATCACTGATGAGCGTTTGGCTCGACAGGAAACCGTGTGGAATATAACACCTAAGAATAT
GTCTGTTACCCATGATATGATGCTTTTTAAGGCCAGCCGGGGAGAAAGGACTGTGTACTCTGTGTGTTG
GGAGGGAGGTGGCAGGTTGAATACTAGGGTTCTGTGA 3`

CYREN
5`
GCAGGCTTCGCCACCATGGAAACCTTACAATCCGAGACTAAAACGAGGGTCCTTCCCTCATGGCTGACA
GCCCAGGTGGCTACAAAGAATGTGGCACCAATGAAGGCCCCCAAGAGGATGAGAATGGCAGCAGTGCC
AGTGGCAGCAGCAAGACTCCCTGCGACAAGGACTGTGTACTGCATGAATGAGGCTGAGATAGTTGATG
TTGCTCTGGGAATCCTGATTGAGAGCCGCAAACAGGAAAAGGCCTGCGAGCAGCCGGCCCTGGCGGGG
GCTGATAACCCAGAGCACTCCCCTCCCTGCTCCGTGTCGCCTCACACAAGTTCTGGGAGCAGCAGTGAG
GAAGAGGACAGTGGGAAACAGGCACTGGCTCCAGGCCTCAGCCCTTCCCAGAGGCCGGGGGGTTCCA

GCTCTGCCTGTAGCAGGAGCCCTGAGGAGGAGGAGGAAGAGGATGTGCTGAAATACGTCCGGGAGAT
CTTTTTCAGCCCGGCGGCTAAAAGAGTTAAACTTGATTAGGACCCAGC 3`

Cry1 without NLS

5`

TCGCCACCATGGGGGTGAACGCCGTGCACTGGTTCCGAAAGGGGCTCCGGCTCCACGACAACCCCGCCC
TGAAGGAGTGCATTCAGGGCGCCGACACCATCCGCTGCGTCTACATCCTGGACCCCTGGTTCGCCGGCT
CCTCCAATGTGGGCATCAACAGGTGGCGATTTTTGCTTCAGTGTCTTGAGGATCTTGATGCCAATCTACG
AAAATTAAACTCCCGTCTGTTTGTGATTCGTGGACAACCAGCAGATGTGTTTCCCAGGCTTTTCAAGGAA
TGGAACATTACTAAACTTTCAATTGAGTATGATTCTGAGCCCTTTGGAAAGGAACGAGACGCAGCTATTA
AGAAACTGGCAACTGAAGCTGGAGTAGAAGTCATTGTAAGAATTTCACATACATTATATGACCTAGACA
AGATCATAGAACTCAATGGTGGACAACCGCCTCTAACTTATAAAAGATTCCAGACTCTCATCAGCAAAAT
GGAACCACTAGAGATACCAGTAGAGACAATTACTTCAGAAGTGATAGAAAAGTGCACAACTCCTCTGTC
TGATGACCATGATGAGAAATATGGAGTCCCTTCACTGGAAGAGCTAGGTTTTGATACAGATGGCTTATC
CTCTGCAGTGTGGCCAGGTGGAGAAACTGAAGCACTTACTCGTTTGGAAAGGCATTTGGAAAGAAAAG
CTTGGGTGGCAAATTTTGAAAGACCTCGAATGAATGCGAATTCTCTGCTTGCAAGCCCTACTGGACTTAG
TCCTTATCTCCGATTTGGTTGTTTGTCATGTCGACTGTTTTACTTCAAACTAACAGATCTCTACAAAAAGGT
AAAGAAGAACAGTTCCCCTCCCCTTTCCCTTTATGGGCAACTGTTATGGCGTGAATTTTTCTATACAGCAG
CAACAAATAATCCACGCTTTGATAAAATGGAAGGAAACCCTATCTGTGTTCAGATTCCTTGGGATAAAAA
TCCTGAGGCTTTAGCCAAATGGGCGGAAGGCCGGACAGGCTTTCCATGGATTGATGCCATCATGACACA
GCTTCGTCAGGAGGGTTGGATTCATCATCTAGCCAGGCATGCAGTTGCTTGCTTCCTGACACGAGGGGA
CCTGTGGATTAGTTGGGAAGAAGGAATGAAGGTATTTGAAGAATTATTGCTTGATGCAGATTGGAGCAT
AAATGCTGGAAGTTGGATGTGGCTGTCTTGTAGTTCCTTTTTTCAACAGTTTTTTCACTGCTATTGCCCTG
TTGGTTTTGGTAGGAGAACAGATCCCAATGGAGACTATATCAGGCGTTATTTGCCTGTCCTAAGAGGCTT
CCCTGCAAAATATATCTATGATCCCTGGAATGCACCAGAAGGTATCCAAAAGGTAGCCAAATGTTTGATA
GGAGTTAATTATCCTAAACCAATGGTGAACCATGCTGAGGCAAGCCGTTTGAATATCGAAAGGATGAAA
CAGATCTATCAGCAGCTTTCACGATATAGAGGACTAGGTCTTCTGGCATCAGTACCTTCTAATCCTAATG
GGAATGGAGGCTTCATGGGATATTCTGCAGAAAATATCCCAGGTTGTAGCAGCAGTGGAAGTTGCTCTC
AAGGGAGTGGTATTTTACACTATGCTCATGGCGACAGTCAGCAAACTCACCTGTTGAAGCAAGGAAGAA

GCTCCATGGGCACTGGTCTCAGTGGTGGGAAACGTCCTAGTCAGGAAGAGGACACACAGAGTATTGGT
CCTAAAGTCCAGAGACAGAGCACTAATTAG 3`

Cry1 5´end NLS

5`

TCGCCACCATGCCGGCGGCTAAAAGAGTTAAACTTGATGGGGTGAACGCCGTGCACTGGTTCCGAAAG
GGGCTCCGGCTCCACGACAACCCCGCCCTGAAGGAGTGCATTCAGGGCGCCGACACCATCCGCTGCGTC
TACATCCTGGACCCCTGGTTCGCCGGCTCCTCCAATGTGGGCATCAACAGGTGGCGATTTTTGCTTCAGT
GTCTTGAGGATCTTGATGCCAATCTACGAAAATTAAACTCCCGTCTGTTTGTGATTCGTGGACAACCAGC
AGATGTGTTTCCCAGGCTTTTCAAGGAATGGAACATTACTAAACTTTCAATTGAGTATGATTCTGAGCCC
TTTGGAAAGGAACGAGACGCAGCTATTAAGAAACTGGCAACTGAAGCTGGAGTAGAAGTCATTGTAAG
AATTTCACATACATTATATGACCTAGACAAGATCATAGAACTCAATGGTGGACAACCGCCTCTAACTTAT
AAAAGATTCCAGACTCTCATCAGCAAAATGGAACCACTAGAGATACCAGTAGAGACAATTACTTCAGAA
GTGATAGAAAAGTGCACAACTCCTCTGTCTGATGACCATGATGAGAAATATGGAGTCCCTTCACTGGAA
GAGCTAGGTTTTGATACAGATGGCTTATCCTCTGCAGTGTGGCCAGGTGGAGAAACTGAAGCACTTACT
CGTTTGGAAAGGCATTTGGAAAGAAAAGCTTGGGTGGCAAATTTTGAAAGACCTCGAATGAATGCGAA
TTCTCTGCTTGCAAGCCCTACTGGACTTAGTCCTTATCTCCGATTTGGTTGTTTGTCATGTCGACTGTTTTA
CTTCAAACTAACAGATCTCTACAAAAAGGTAAAGAAGAACAGTTCCCCTCCCCTTTCCCTTTATGGGCAA
CTGTTATGGCGTGAATTTTTCTATACAGCAGCAACAAATAATCCACGCTTTGATAAAATGGAAGGAAACC
CTATCTGTGTTCAGATTCCTTGGGATAAAAATCCTGAGGCTTTAGCCAAATGGGCGGAAGGCCGGACAG
GCTTTCCATGGATTGATGCCATCATGACACAGCTTCGTCAGGAGGGTTGGATTCATCATCTAGCCAGGCA
TGCAGTTGCTTGCTTCCTGACACGAGGGGACCTGTGGATTAGTTGGGAAGAAGGAATGAAGGTATTTG
AAGAATTATTGCTTGATGCAGATTGGAGCATAAATGCTGGAAGTTGGATGTGGCTGTCTTGTAGTTCCTT
TTTTCAACAGTTTTTTCACTGCTATTGCCCTGTTGGTTTTGGTAGGAGAACAGATCCCAATGGAGACTATA
TCAGGCGTTATTTGCCTGTCCTAAGAGGCTTCCCTGCAAAATATATCTATGATCCCTGGAATGCACCAGA
AGGTATCCAAAAGGTAGCCAAATGTTTGATAGGAGTTAATTATCCTAAACCAATGGTGAACCATGCTGA
GGCAAGCCGTTTGAATATCGAAAGGATGAAACAGATCTATCAGCAGCTTTCACGATATAGAGGACTAGG
TCTTCTGGCATCAGTACCTTCTAATCCTAATGGGAATGGAGGCTTCATGGGATATTCTGCAGAAAATATC
CCAGGTTGTAGCAGCAGTGGAAGTTGCTCTCAAGGGAGTGGTATTTTACACTATGCTCATGGCGACAGT

CAGCAAACTCACCTGTTGAAGCAAGGAAGAAGCTCCATGGGCACTGGTCTCAGTGGTGGGAAACGTCC
TAGTCAGGAAGAGGACACACAGAGTATTGGTCCTAAAGTCCAGAGACAGAGCACTAATTAG 3`

Cry1 3´end NLS

5`

ACTTTGTACAAAAAAGCAGGCTTCGCCACCATGGGGGTGAACGCCGTGCACTGGTTCCGAAAGGGGCT
CCGGCTCCACGACAACCCCGCCCTGAAGGAGTGCATTCAGGGCGCCGACACCATCCGCTGCGTCTACAT
CCTGGACCCCTGGTTCGCCGGCTCCTCCAATGTGGGCATCAACAGGTGGCGATTTTTGCTTCAGTGTCTT
GAGGATCTTGATGCCAATCTACGAAAATTAAACTCCCGTCTGTTTGTGATTCGTGGACAACCAGCAGATG
TGTTTCCCAGGCTTTTCAAGGAATGGAACATTACTAAACTTTCAATTGAGTATGATTCTGAGCCCTTTGGA
AAGGAACGAGACGCAGCTATTAAGAAACTGGCAACTGAAGCTGGAGTAGAAGTCATTGTAAGAATTTC
ACATACATTATATGACCTAGACAAGATCATAGAACTCAATGGTGGACAACCGCCTCTAACTTATAAAAGA
TTCCAGACTCTCATCAGCAAAATGGAACCACTAGAGATACCAGTAGAGACAATTACTTCAGAAGTGATA
GAAAAGTGCACAACTCCTCTGTCTGATGACCATGATGAGAAATATGGAGTCCCTTCACTGGAAGAGCTA
GGTTTTGATACAGATGGCTTATCCTCTGCAGTGTGGCCAGGTGGAGAAACTGAAGCACTTACTCGTTTG
GAAAGGCATTTGGAAAGAAAAGCTTGGGTGGCAAATTTTGAAAGACCTCGAATGAATGCGAATTCTCTG
CTTGCAAGCCCTACTGGACTTAGTCCTTATCTCCGATTTGGTTGTTTGTCATGTCGACTGTTTTACTTCAAA
CTAACAGATCTCTACAAAAAGGTAAAGAAGAACAGTTCCCCTCCCCTTTCCCTTTATGGGCAACTGTTAT
GGCGTGAATTTTTCTATACAGCAGCAACAAATAATCCACGCTTTGATAAAATGGAAGGAAACCCTATCTG
TGTTCAGATTCCTTGGGATAAAAATCCTGAGGCTTTAGCCAAATGGGCGGAAGGCCGGACAGGCTTTCC
ATGGATTGATGCCATCATGACACAGCTTCGTCAGGAGGGTTGGATTCATCATCTAGCCAGGCATGCAGT
TGCTTGCTTCCTGACACGAGGGGACCTGTGGATTAGTTGGGAAGAAGGAATGAAGGTATTTGAAGAAT
TATTGCTTGATGCAGATTGGAGCATAAATGCTGGAAGTTGGATGTGGCTGTCTTGTAGTTCCTTTTTTCA
ACAGTTTTTTCACTGCTATTGCCCTGTTGGTTTTGGTAGGAGAACAGATCCCAATGGAGACTATATCAGG
CGTTATTTGCCTGTCCTAAGAGGCTTCCCTGCAAAATATATCTATGATCCCTGGAATGCACCAGAAGGTA
TCCAAAAGGTAGCCAAATGTTTGATAGGAGTTAATTATCCTAAACCAATGGTGAACCATGCTGAGGCAA
GCCGTTTGAATATCGAAAGGATGAAACAGATCTATCAGCAGCTTTCACGATATAGAGGACTAGGTCTTC
TGGCATCAGTACCTTCTAATCCTAATGGGAATGGAGGCTTCATGGGATATTCTGCAGAAAATATCCCAG
GTTGTAGCAGCAGTGGAAGTTGCTCTCAAGGGAGTGGTATTTTACACTATGCTCATGGCGACAGTCAGC
AAACTCACCTGTTGAAGCAAGGAAGAAGCTCCATGGGCACTGGTCTCAGTGGTGGGAAACGTCCTAGTC

AGGAAGAGGACACACAGAGTATTGGTCCTAAAGTCCAGAGACAGAGCACTAATCCGGCGGCTAAAAGA
GTTAAACTTGATTAGGACCCAGCTTTCTTGTACAAAG 3`